
Detecting Adversarial Data by Probing Multiple Perturbations Using Expected Perturbation Score

Shuhai Zhang^{*12} Feng Liu^{*3} Jiahao Yang¹ Yifan Yang¹ Changsheng Li⁴ Bo Han⁵ Mingkui Tan¹⁶

Abstract

Adversarial detection aims to determine whether a given sample is an adversarial one based on the discrepancy between natural and adversarial distributions. Unfortunately, estimating or comparing two data distributions is extremely difficult, especially in high-dimension spaces. Recently, the *gradient* of log probability density (a.k.a., score) w.r.t. the sample is used as an alternative statistic to compute. However, we find that the score is sensitive in identifying adversarial samples due to insufficient information with one sample only. In this paper, we propose a new statistic called *expected perturbation score* (EPS), which is essentially the expected score of a sample after various perturbations. Specifically, to obtain adequate information regarding one sample, we perturb it by adding various noises to capture its multi-view observations. We theoretically prove that EPS is a proper statistic to compute the discrepancy between two samples under mild conditions. In practice, we can use a pre-trained diffusion model to estimate EPS for each sample. Last, we propose an EPS-based adversarial detection (EPS-AD) method, in which we develop EPS-based *maximum mean discrepancy* (MMD) as a metric to measure the discrepancy between the test sample and natural samples. We also prove that the EPS-based MMD between natural and adversarial samples is larger than that among natural samples. Extensive experiments show the superior adversarial detection performance of our EPS-AD.

1. Introduction

Deep neural networks (DNNs) are known to be sensitive to adversarial samples that are generated by adding imperceptible perturbations to the input but may mislead the model to make unexpected predictions (Szegedy et al., 2014; Goodfellow et al., 2015; Niu et al., 2022; 2023; Li et al., 2023). Adversarial samples threaten widespread machine learning systems (Li & Vorobeychik, 2014; Ozbulak et al., 2019), which raises an urgent requirement for advanced techniques to improve the robustness of models. Among them, *adversarial training* introduces adversarial data into training to improve the robustness of models but suffers from significant performance degradation and high computational complexity (Laidlaw et al., 2021; Wong et al., 2020); *adversarial purification* relies on generative models to purify adversarial data before classification, which still has to compromise on unsatisfactory natural and adversarial accuracy (Shi et al., 2021; Yoon et al., 2021; Nie et al., 2022).

In contrast, another class of defense methods, called *adversarial detection*, could be achieved by detecting and rejecting adversarial examples, which are friendly to existing machine learning systems due to the almost lossless natural accuracy, and can help to identify security-compromised input sources (Abusnaina et al., 2021). Adversarial detection aims to tell whether a test sample is an adversarial sample, for which the key is to find the discrepancy between the adversarial and natural distributions. However, existing adversarial detection approaches primarily train a tailored detector for specific attacks (Feinman et al., 2017; Ma et al., 2018; Lee et al., 2018) or for a specific classifier (Deng et al., 2021), which largely overlook modeling the adversarial and natural distributions, resulting in their limited performance against unseen attacks or transferable attacks.

Unfortunately, it is non-trivial to estimate or compare two data distributions, especially in high-dimension spaces. One alternative approach is to estimate the *gradient* of log probability density with respect to the sample, *i.e.*, score. This statistic has emerged as a powerful means for adversarial defense (Yoon et al., 2021; Nie et al., 2022) and diffusion models (Song & Ermon, 2019; Song et al., 2021; Huang et al., 2021). However, how to effectively exploit the score function for adversarial detection is not well studied.

^{*}Equal contribution ¹School of Software Engineering, South China University of Technology, China ²Pazhou Laboratory, China ³The University of Melbourne ⁴Beijing Institute of Technology, Beijing, China ⁵Department of Computer Science, Hong Kong Baptist University ⁶Key Laboratory of Big Data and Intelligent Robot, Ministry of Education, China. Correspondence to: Mingkui Tan <mingkui-tan@scut.edu.cn>, Bo Han <bhanml@comp.hkbu.edu.hk>, Changsheng Li <lcs@bit.edu.cn>.

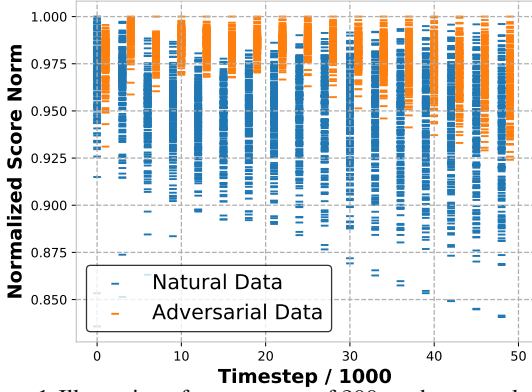


Figure 1. Illustration of score norms of 200 random sampled natural and adversarial images on ImageNet, where most natural images have lower norms than adversarial ones at the same timestep but are sensitive to the timesteps due to the significant overlap.

Recently, Yoon et al. (2021) purify adversarial samples by gradually removing the adversarial noise from the (attacked) samples with the score function for adversarial defense. During the purification process, they employ the *norm* of scores (between being-purified adversarial samples and natural samples) to set a threshold for determining which timestep to stop purifying. They empirically find that natural samples usually have lower score norms than adversarial samples across purification timesteps. Intuitively, the score could represent the momentum of the sample towards the high-density areas of natural data (Song & Ermon, 2019). This means that a lower score norm indicates the sample is closer to the high-density areas of natural data, *i.e.*, a higher probability of the sample following the natural distribution. To further understand this, we demonstrate the score norms of natural and adversarial samples at different purification timesteps. According to Figure 1, most natural samples have lower score norms than adversarial samples at the same timestep, but they are very sensitive to the timesteps due to the significant overlap across all timesteps. This suggests that the score of one sample is useful but not effective enough in identifying the adversarial samples.

To address the above issue, we propose a new statistic called *expected perturbation score* (EPS), which represents the expected score after multiple perturbations of a given sample. In EPS, we consider multiple levels of noise perturbations to diversify one sample, allowing us to capture multi-view observations of one sample and thus extract adequate information from the data. Our theoretical analysis shows EPS is a valid statistic in distinguishing between natural and adversarial samples under mild conditions. Thus, we propose an *EPS-based adversarial detection* method (EPS-AD) for adversarial detection, as illustrated in Figure 2. Specifically, given a pre-trained score-based diffusion model, EPS-AD consists of three steps: 1) we simultaneously add multiple perturbations to a set of natural images and a test image following the forward diffusion process with a time step T^* ;

2) we obtain their EPSs via the score model; 3) we adopt the *maximum mean discrepancy* (MMD) between any test sample and natural samples relying on EPS. Theoretical and empirical evidences show the superiority of our method.

We summarize our main contributions as follows:

- A novel statistic. We find that the traditional score of one sample is sensitive in identifying adversarial samples due to insufficient information from a single sample only. However, we can perturb the sample by adding various noises and thus can obtain various information from its multi-view observations or perturbations. We propose to calculate the expected score of the multiple perturbations of the sample, namely *expected perturbation score* (EPS). This new statistic can be much more reliable and effective than traditional score (*e.g.*, Yoon et al. (2021)) in measuring the distributional discrepancy.
- A novel adversarial detection method with extensive empirical justifications. Based on the novel statistic EPS, we further develop a novel single-sample adversarial detection method called EPS-AD, in which we propose an EPS-based *maximum mean discrepancy* (MMD) and then use it as a metric to measure the discrepancy between the test sample and natural samples. We conduct extensive experiments on both CIFAR-10 and ImageNet across various network architectures, including ResNet, WideResNet and ViT. Our method consistently outperforms existing methods against 12 different attacks.
- Theoretical justifications. First, we provide theoretical analysis that EPS is a proper statistic to distinguish between natural and adversarial data well under mild conditions (Theorem 1). Specifically, we show that the EPS of the natural sample is closer to those of other natural samples compared to adversarial samples. Second, we theoretically show that the EPS-based MMD between natural and adversarial samples is larger than that among natural samples (Corollary 1).

2. Preliminaries

Adversarial data generation. Given a well-trained classifier \hat{f} on a data set $D = \{(\mathbf{x}_i, l_i)\}_{i=1}^n$ with \mathbf{x}_i being a sample from the input space \mathcal{X} and l_i being its ground-truth label defined in a label set $\mathcal{C} = \{1, \dots, C\}$, adversarial data $\hat{\mathbf{x}}$ regarding \mathbf{x} with perturbation ϵ is given by

$$\hat{\mathbf{x}} = \arg \max_{\hat{\mathbf{x}} \in \mathcal{B}(\mathbf{x}, \epsilon)} \ell(\hat{f}(\hat{\mathbf{x}}), l), \quad (1)$$

where $\mathcal{B}(\mathbf{x}, \epsilon) = \{\mathbf{x}' \in \mathcal{X} \mid d(\mathbf{x}, \mathbf{x}') \leq \epsilon\}$, d is some distance (*e.g.*, l_2 or l_∞ distance), and ℓ is some loss function. For simplicity, we denote $\hat{\mathbf{x}} = \mathbf{x} + \epsilon$ as the adversarial data.

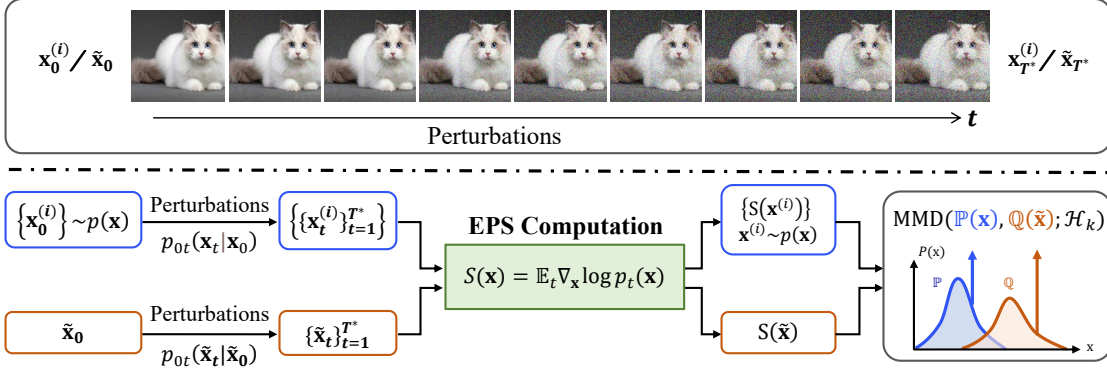


Figure 2. Overview of the proposed EPS-AD. EPS denotes the expected score after multiple perturbations of a sample using a pre-trained score model. Specifically, we simultaneously add perturbations to a set of natural images $\{\mathbf{x}_0^{(i)}\}$ and a test image $\tilde{\mathbf{x}}_0$ following the diffusion process with a time step T^* to get perturbed images, from which we obtain their EPSs $S(\mathbf{x})$ via the score model and calculate the MMD between EPS of the test sample and EPSs of natural samples.

Continuous-time diffusion models. Following Song et al. (2021), let $p(\mathbf{x})$ be the unknown data distribution. Diffusion models firstly construct a forward diffusion process $\{\mathbf{x}_t\}_{t=0}^{T_{\text{diff}}}$ indexed by a continuous time variable $t \in [0, T_{\text{diff}}]$, which can be modeled by a stochastic differential equation (SDE) with positive time increments:

$$d\mathbf{x} = \mathbf{f}(\mathbf{x}, t)dt + g(t)d\mathbf{w}, \quad (2)$$

where $\mathbf{x}_0 := \mathbf{x} \sim p(\mathbf{x})$, $\mathbf{f}(\cdot, t) : \mathbb{R}^d \rightarrow \mathbb{R}^d$ is a vector-valued function, $g(\cdot) : \mathbb{R} \rightarrow \mathbb{R}$ is a scalar function that is independent of \mathbf{x} , and \mathbf{w} is a standard Wiener process.

Let $p_t(\mathbf{x})$ be the the marginal distribution of \mathbf{x}_t with $p_0(\mathbf{x}) = p(\mathbf{x})$, if $\mathbf{f}(\mathbf{x}, t)$ and $g(t)$ are designed well such that $p_T(\mathbf{x}) \approx \mathcal{N}(\mathbf{0}, \mathbf{I}_d)$, by reversing the diffusion process from $t = T_{\text{diff}}$ to $t = 0$, we can reconstruct samples $\mathbf{x}_0 \sim p_0(\mathbf{x})$. The reverse process is given by the reverse-time SDE:

$$d\mathbf{x} = [\mathbf{f}(\mathbf{x}, t) - g(t)^2 \nabla_{\mathbf{x}} \log p_t(\mathbf{x})] dt + g(t)d\bar{\mathbf{w}}, \quad (3)$$

where $\bar{\mathbf{w}}$ is a standard reverse-time Wiener process and dt is an infinitesimal negative time step. Throughout the paper, we consider the VP-SDE following the setting of Song et al. (2021), where $\mathbf{f}(\mathbf{x}, t) := -\frac{1}{2}\beta(t)\mathbf{x}$ and $g(t) := \sqrt{\beta(t)}$ with $\beta(t)$ being the linear noise schedule, i.e., $\beta(t) := \beta_{\min} + (\beta_{\max} - \beta_{\min})t/T_{\text{diff}}$ for $t \in [0, T_{\text{diff}}]$.

Reconstructing samples from the Gaussian distribution requires the score of the marginal distribution, i.e., $\nabla_{\mathbf{x}} \log p_t(\mathbf{x})$ in the reverse process Eq. (3). To estimate the score function $\nabla_{\mathbf{x}} \log p_t(\mathbf{x})$, one effective solution is to train a score model $s_{\theta}(\mathbf{x}, t)$ on samples with score matching (Hyvärinen & Dayan, 2005; Song & Ermon, 2019; Vincent, 2011). The training objective function is minimizing:

$$\mathbb{E}_t \left[\lambda(t) \mathbb{E}_{p_0(\mathbf{x}_0)p_{0t}(\mathbf{x}_t|\mathbf{x}_0)} \|s_{\theta}(\mathbf{x}_t, t) - \nabla_{\mathbf{x}_t} \log p_{0t}(\mathbf{x}_t|\mathbf{x}_0)\|_2^2 \right], \quad (4)$$

where $\lambda(t)$ is a weight w.r.t. t and $p_{0t}(\mathbf{x}_t | \mathbf{x}_0)$ is a transition kernel from \mathbf{x}_0 to \mathbf{x}_t that can be derived by Eq. (2).

Maximum mean discrepancy. Following Gretton et al. (2012); Borgwardt et al. (2006), let $\mathcal{X} \subset \mathbb{R}^d$ be a separable metric space and p, q be Borel probability measures on \mathcal{X} . Given two independent identically distributed (IID) observations $S_X = \{\mathbf{x}^{(i)}\}_{i=1}^n$ and $S_Y = \{\mathbf{y}^{(i)}\}_{i=1}^m$ from distributions p and q , respectively, *maximum mean discrepancy* (MMD) aims to measure the closeness between these two distributions, which is defined as:

$$\text{MMD}(p, q; \mathcal{F}) := \sup_{f \in \mathcal{F}} |\mathbb{E}[f(X)] - \mathbb{E}[f(Y)]|, \quad (5)$$

where \mathcal{F} is a class of functions $f : \mathcal{X} \rightarrow \mathbb{R}$, and $X \sim p, Y \sim q$ are two random variables. To better study the richness of the MMD function class \mathcal{F} , Borgwardt et al. (2006) propose to choose \mathcal{F} to be the unit ball in a universal reproducing kernel Hilbert space and obtain the following kernel-based MMD,

$$\begin{aligned} \text{MMD}(p, q; \mathcal{H}_k) &:= \sup_{f \in \mathcal{H}_k, \|f\|_{\mathcal{H}_k} \leq 1} |\mathbb{E}[f(X)] - \mathbb{E}[f(Y)]| \\ &= \|\mu_p - \mu_q\|_{\mathcal{H}_k} = \sqrt{\mathbb{E}[k(X, X') + k(Y, Y') - 2k(X, Y)]}, \end{aligned} \quad (6)$$

where $k : \mathcal{X} \times \mathcal{X} \rightarrow \mathbb{R}$ is the kernel of a reproducing kernel Hilbert space \mathcal{H}_k , $\mu_p := \mathbb{E}[k(\cdot, X)]$ and $\mu_q := \mathbb{E}[k(\cdot, Y)]$ are the kernel mean embeddings of p and q , respectively (Gretton et al., 2012; Borgwardt et al., 2006; Jitkrittum et al., 2017; Liu et al., 2020; Gao et al., 2021). In addition, Liu et al. (2020) propose deep-kernel-based MMD to select the adaptive kernel for two-sample tests.

Adversarial detection. In this paper, we aim to address the following adversarial detection problem.

Problem 1. Let $\mathcal{X} \subset \mathbb{R}^d$ be a separable metric space and p be a Borel probability measure on \mathcal{X} , and IID observations $S_X = \{\mathbf{x}^{(i)}\}_{i=1}^n$ from the distribution p and a ground-truth labeling mapping $f : \mathbb{R}^d \rightarrow \mathcal{C}$ with $\mathcal{C} = \{1, \dots, C\}$ being a label set. Assuming that the attacker has access to some well-trained classifier \hat{f} on S_X and IID observations S'_X

from the distribution p , we wish to know whether each new sample in $S_Y = \{\mathbf{y}^{(i)}\}_{i=1}^m$ that are crafted with S'_X is following the distribution p .

Note that the definition of *adversarial detection* in Problem 1 is different from that in two-sample test (Grosse et al., 2017). Particularly, Problem 1 aims to determine whether each example in S_Y is sampled from the distribution p , while two-sample test aims to tell if two populations S_X and S_Y come from the same distribution, which focuses on the closeness between two populations.

3. Expected Perturbation Score for Adversarial Detection

Existing methods (e.g., Yoon et al. (2021)) seek to use the score (the gradient of log probability density w.r.t. the sample) of one sample to measure the discrepancy between natural and adversarial distributions for adversarial detection. However, this measure is not accurate enough for detecting a single test sample, as the insufficient information available for a single sample can result in highly fluctuating distributional discrepancies. Moreover, although they have empirically demonstrated some results about the norm of score in distinguishing adversarial samples from natural samples, yet do not provide deep investigations or theoretical analysis on it.

To address the above issues, we consider obtaining more information of a sample using its multi-view perturbations and propose a new statistic called **expected perturbation score** (EPS) to measure the distributional discrepancy (Section 3.1). Based on this new statistic, we develop an **EPS-based adversarial detection** method, called EPS-AD, as shown in Figure 2. Particularly, we estimate the EPS for each sample using a pre-trained diffusion model, then adopt the *maximum mean discrepancy* (MMD) between the test sample and a set of natural samples relying on EPS as a characteristic of the test sample for adversarial detection (Section 3.2). Last, we provide theoretical analyses that the MMD between EPSs of the natural samples is smaller than that between natural and adversarial samples (Section 3.3).

3.1. Expected Perturbation Score

To begin with, we provide the definition of *expected perturbation score* (EPS) to develop our proposed method.

Definition 1. (Expected perturbation score) Let $\mathcal{X} \subset \mathbb{R}^d$ be a separable metric space and p be Borel probability measure on \mathcal{X} . Given a perturbation process transition distribution $p_{0t}(\mathbf{x}_t | \mathbf{x}_0)$ from \mathbf{x}_0 to \mathbf{x}_t , the *expected perturbation score* (EPS) of a sample $\mathbf{x} \sim p$ is given by:

$$S(\mathbf{x}) = \mathbb{E}_{t \sim U(0,T)} \nabla_{\mathbf{x}} \log p_t(\mathbf{x}), \quad (7)$$

where $p_t(\mathbf{x})$ is the marginal probability distribution of \mathbf{x}_t

with $p_0(\mathbf{x}) := p(\mathbf{x})$ and T is the last perturbation timestep.

Remark 1. Note that the perturbation process transition distribution $p_{0t}(\mathbf{x}_t | \mathbf{x}_0)$ can be any distribution, such as Gaussian distribution or uniform distribution. Moreover, unlike only computing a single score of one sample proposed by Song et al. (2021), we incorporate multiple levels of noise through $p_{0t}(\mathbf{x}_t | \mathbf{x}_0)$ at different timesteps t in the definition of EPS, with the aim of diversifying the single sample, which enables us to capture multi-view observation data and thus fully exploit more information from the data.

Built upon Definition 1, we derive a following theorem to give a closer look on EPS $S(\mathbf{x})$ for the natural and adversarial data when the perturbation process transition distribution $p_{0t}(\mathbf{x}_t | \mathbf{x}_0)$ and $p(\mathbf{x})$ are from Gaussian distributions.

Theorem 1. Assuming that the distribution of natural data $p(\mathbf{x}) = \mathcal{N}(\boldsymbol{\mu}_x, \sigma_x^2 \mathbf{I})$, where \mathbf{I} is an identity matrix, given a perturbation transition kernel $p_{0t}(\mathbf{x}_t | \mathbf{x}_0) = \mathcal{N}(\gamma_t \mathbf{x}_0, \sigma_t^2 \mathbf{I})$ with γ_t and σ_t being the time-dependent noise schedule, then the following three conclusions hold:

- 1) For $\forall \mathbf{x} \sim p(\mathbf{x})$, $S(\mathbf{x}) \sim \mathcal{N}(\mathbf{0}, \sigma_S^2 \mathbf{I})$;
- 2) For $\forall \mathbf{y} \sim p(\mathbf{x})$ and adversarial sample $\hat{\mathbf{y}} = \mathbf{y} + \boldsymbol{\varepsilon}$, $S(\hat{\mathbf{y}}) \sim \mathcal{N}(-\boldsymbol{\mu}_S, \sigma_S^2 \mathbf{I})$;
- 3) For $\forall \mathbf{x}, \mathbf{y} \sim p(\mathbf{x})$ and adversarial sample $\hat{\mathbf{y}} = \mathbf{y} + \boldsymbol{\varepsilon}$,

$$S(\mathbf{x}) - S(\mathbf{y}) \sim \mathcal{N}(\mathbf{0}, 2\sigma_S^2 \mathbf{I}); \quad (8)$$

$$S(\mathbf{x}) - S(\hat{\mathbf{y}}) \sim \mathcal{N}(\boldsymbol{\mu}_S, 2\sigma_S^2 \mathbf{I}), \quad (9)$$

where $\boldsymbol{\mu}_S = \mathbb{E}_{t \sim U(0,T)} \boldsymbol{\mu}_t$ with $\boldsymbol{\mu}_t = \frac{\boldsymbol{\varepsilon}}{\gamma_t^2 \sigma_x^2 + \sigma_t^2}$ and $\sigma_S^2 = \mathbb{E}_{t \sim U(0,T)} \zeta_t^2$ with $\zeta_t^2 = \frac{1}{\gamma_t^2 \sigma_x^2 + \sigma_t^2}$.

Remark 2. Note that analyzing scores (i.e., gradients of log probability) under complex practical distributions can be very difficult and infeasible. Nevertheless, we still hope to deeply investigate our EPS from a theoretical perspective and see whether it has some advantages over existing ones in theory. To this end, we adopt a common practice by assuming that the data follows some Gaussian distribution.

Theorem 1 tells us: 1) the first two findings show that the mean of EPS for the adversarial sample differs from that of the natural sample due to the additional term $\boldsymbol{\mu}_S$; 2) the third finding indicates that the EPS of the natural sample is closer to that of other natural samples compared to adversarial samples, and this discrepancy becomes more pronounced when the perturbation transitions γ_t and σ_t are small. This motivates us to employ $S(\mathbf{x})$ for adversarial detection.

Necessity of multiple scores in EPS. Note that ζ_t^2 and $\|\boldsymbol{\mu}_t\|^2$ decrease as the timestep t increases due to the increase of γ_t and σ_t . However, smaller variance σ_S^2 and larger mean $\|\boldsymbol{\mu}_S\|^2$ are required for good adversarial detection. If we only consider one score of some unique timestep t (i.e., removing the expectation from the definition of EPS), the variance σ_S^2 and mean $\boldsymbol{\mu}_S$ of the discrepancy will be so

fluctuant that performing detecting adversarial samples will be very sensitive to the timestep t (as validated in Figure 1 and Section 4.4). To alleviate this issue, we consider taking expectation w.r.t. the timestep on multiple scores. In this way, the distribution of the discrepancy between the natural sample and the adversarial sample will be more stable to the timestep, which makes it easier to obtain a superior solution.

Estimation for EPS. Note that EPS (*i.e.*, $S(\mathbf{x})$) in Eq. (7) requires knowing the score function $\nabla_{\mathbf{x}} \log p_t(\mathbf{x})$, which can be estimated by training a neural network with score matching (Song & Ermon, 2019; Vincent, 2011). To this end, we model the perturbation process transition as a Gaussian distribution $p_{0t}(\mathbf{x}_t | \mathbf{x}_0) = \mathcal{N}(\gamma_t \mathbf{x}_0, \sigma_t^2 \mathbf{I})$, where $\gamma_t = e^{-\frac{1}{2} \int_0^t \beta(s) ds}$ and $\sigma_t^2 = 1 - e^{-\int_0^t \beta(s) ds}$ with $\beta(t)$ for $t \in [0, 1000]$ being the time-dependent noise schedule. By optimizing Eq. (4), with sufficient data and model capacity, score matching ensures that the optimal solution to Eq. (4) equals $\nabla_{\mathbf{x}} \log p_t(\mathbf{x})$ for almost \mathbf{x} and t (Song et al., 2021). As a result, the score $\nabla_{\mathbf{x}} \log p_t(\mathbf{x})$ can be approximated by $s_{\theta}(\mathbf{x}_t, t)$. In practice, we use a pre-trained diffusion model to achieve the estimation for the score $s_{\theta}(\mathbf{x}_t, t)$.

3.2. Exploring EPS for Adversarial Detection

Using the norm of estimated EPS $S(\mathbf{x})$ as a characterization for adversarial detection is straightforward. Nevertheless, this manner can only describe the magnitude of the EPS vector, so it ignores the rich information that can be derived from its direction. It is critical that we design a distance metric to measure the distance between the EPS of a test sample and the EPSs of natural samples in order to derive more useful information from $S(\mathbf{x})$. To this end, we propose an EPS-based adversarial detection method (EPS-AD) with *maximum mean discrepancy* (MMD).

Benefiting from the superior performance of MMD in measuring two given distributions (Long et al., 2015; Zhu et al., 2019), we resort to it for characterizing EPS. The basic idea of MMD is that two distributions would be identical if two random variables have identical moments for any order, and the moment that makes the largest distance between the two distributions should be the measure of the two distributions when the two distributions are not the same (Gong et al., 2022). To formalize our approach, we consider two sample sets: $\mathbb{P}_X = \{\mathbf{x}^{(i)}\}_{i=1}^n$ for natural samples and $\mathbb{Q}_Y = \{\tilde{\mathbf{x}}\}$ for a test sample. Employing the MMD, we estimate the distance between \mathbb{P}_X and \mathbb{Q}_Y as follows:

$$\begin{aligned} \widehat{\text{MMD}}_b^2[\mathbb{P}_X, \mathbb{Q}_Y; \mathcal{H}_k] &= \frac{1}{n^2} \sum_{i,j=1}^n k(S(\mathbf{x}^{(i)}), S(\mathbf{x}^{(j)})) \\ &\quad - \frac{2}{n} \sum_{i=1}^n k(S(\mathbf{x}^{(i)}), S(\tilde{\mathbf{x}})) + k(S(\tilde{\mathbf{x}}), S(\tilde{\mathbf{x}})), \end{aligned} \quad (10)$$

where k is the kernel of a reproducing kernel Hilbert space \mathcal{H}_k such as the Gaussian kernel $k(\mathbf{a}, \mathbf{b}) = \exp(-\|\mathbf{a} - \mathbf{b}\|^2 / (2\sigma^2))$. In practice, we consider deep kernel MMD for our method following Liu et al. (2020) and refer readers to Supplementary D.1 for more details. In this way, we can obtain a distance between the test sample and a set of natural samples for adversarial detection.

3.3. Theoretical Analysis for EPS-AD

Note that after performing the same perturbation process, the first and the third terms in Eq. (10) are the same for each test sample in most cases such as k is the Gaussian kernel, thus we only focus on the cross-term $J = \frac{2}{n} \sum_{i=1}^n k(S(\mathbf{x}^{(i)}), S(\tilde{\mathbf{x}}))$ for the test sample.

Corollary 1. *Considering the Gaussian kernel $k(\mathbf{a}, \mathbf{b}) = \exp(-\|\mathbf{a} - \mathbf{b}\|^2 / (2\sigma^2))$ and the assumption in Theorem 1, for $\forall 0 < \eta < 1$, the probability of $P\{k(S(\mathbf{x}), S(\tilde{\mathbf{y}})) > \eta\}$ is given by*

$$P\{k(S(\mathbf{x}), S(\tilde{\mathbf{y}})) > \eta\} = \int_0^C \chi_d^2(z) dz, \quad (11)$$

where $z = \|\boldsymbol{\mu}_S\|^2$ with $\boldsymbol{\mu}_S$ being the mean of $S(\mathbf{x}) - S(\tilde{\mathbf{y}})$, C is a constant for given η and σ , χ^2 is the probability density function of noncentral chi-squared distribution with d degrees of freedom (Abdel-Aty, 1954).

Corollary 1 indicates that the cross-term J will be larger if $\|\boldsymbol{\mu}_S\|^2$ is close to zero given an η . Combining Eq. (8) and Eq. (9), we conclude that the natural data have larger J than the adversarial data with higher probability due to the additional term $\mathbb{E}_t \frac{\epsilon}{\gamma_t^2 \sigma_x^2 + \sigma_t^2}$, suggesting that the MMD between EPSs of the natural samples is smaller than that between natural and adversarial samples.

4. Experiments

In this section, we start by providing experimental settings (Section 4.1). Based on various strong attack benchmarks, we then compare our method with state-of-the-art adversarial detection approaches (Sections 4.2 and 4.3). Additionally, we conduct various ablation studies for further understanding of our approach (Section 4.4). Our code is available at <https://github.com/ZSHsh98/EPS-AD.git>.

4.1. Experimental Settings

Datasets and network architectures. We evaluate our method on CIFAR-10 (Krizhevsky, 2009) and ImageNet (Deng et al., 2009). We implement three widely used architectures as classifiers: WideResNet (Zagoruyko & Komodakis, 2016; Goyal et al., 2021) for CIFAR-10, ResNet (He et al., 2016) and ViT (Dosovitskiy et al., 2021)

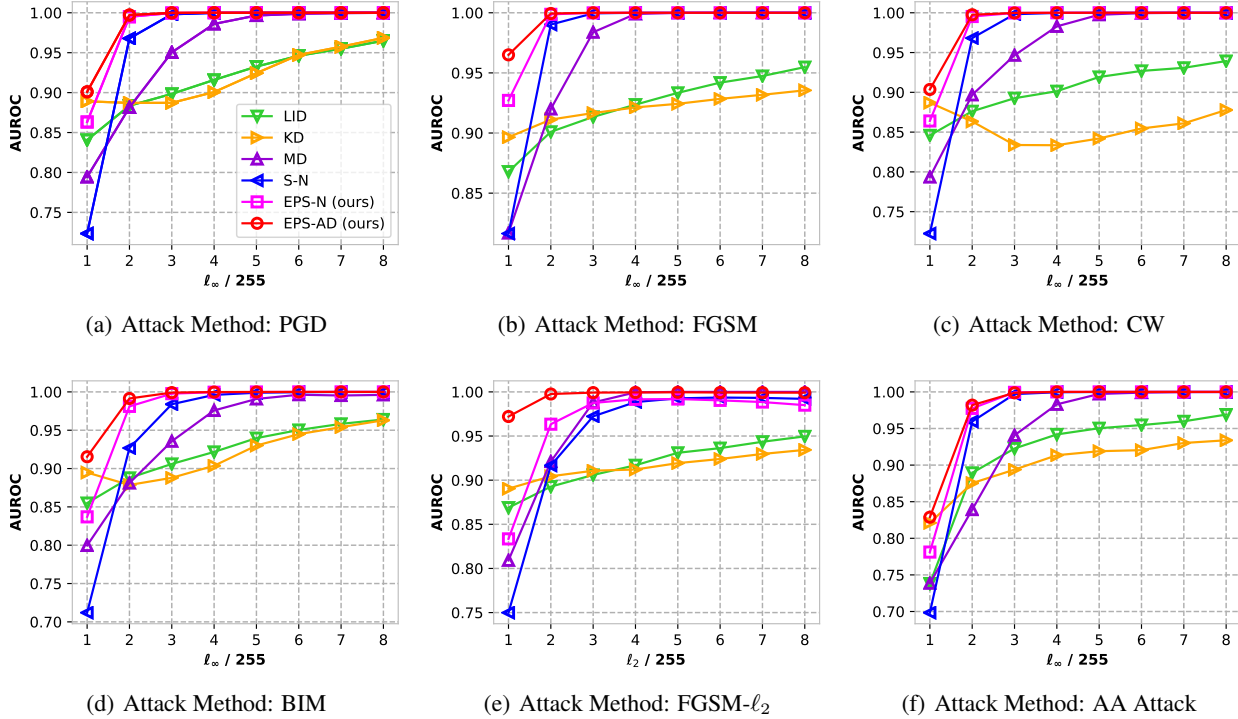


Figure 3. Comparison with adversarial detection methods on CIFAR-10 in terms of AUROC under $\epsilon \in \{1/255, \dots, 8/255\}$ against PGD, FGSM, CW, BIM, FGSM- l_2 , AA. Sub-figures (a) - (f) share the same legend presented in sub-figure (a).

Table 1. Comparison of different adversarial detection methods on CIFAR-10 in terms of AUROC under $\epsilon = 4/255$. The bold number indicates the best results.

AUROC	FGSM	PGD	BIM	CW	FGSM- l_2	BIM- l_2	AA
KD	0.9213	0.9007	0.9037	0.8335	0.9121	0.9107	0.9135
LID	0.9236	0.9159	0.9217	0.9014	0.9169	0.9320	0.9419
MD	0.9990	0.9860	0.9758	0.9829	0.9995	0.9586	0.9830
S-N	1.0000	0.9998	0.9961	0.9998	0.9885	0.9674	0.9995
EPS-N (Ours)	1.0000	1.0000	0.9996	1.0000	0.9916	0.9883	1.0000
EPS-AD (Ours)	1.0000	1.0000	0.9998	1.0000	0.9995	0.9991	1.0000

for ImageNet. For diffusion models, we consider the pre-trained diffusion models of Score SDE (Song et al., 2021) for CIFAR-10 and Guided Diffusion (Dhariwal & Nichol, 2021) for ImageNet, respectively.

Attack methods. Following Deng et al. (2021), we evaluate our adversarial detection method under various attack methods. We consider the commonly used l_2 and l_∞ threat models, including PGD (Madry et al., 2018), FGSM (Goodfellow et al., 2015), BIM (Kurakin et al., 2018), MIM (Dong et al., 2018), TIM (Dong et al., 2019), CW (Carlini & Wagner, 2017), DLMIM(Xie et al., 2019). Moreover, we apply two adaptive attack methods such as AutoAttack (AA) (Croce & Hein, 2020) and Minimum-Margin Attack (MM) (Gao et al., 2022). To show the superiority of our method, we consider the relatively low attack intensities, *i.e.*, l_2 -ball and l_∞ -ball with $\epsilon = 4/255$, and iterative attacks run for 5 steps using step size $\epsilon/5$, unless stated otherwise.

Baselines. We compare our method with several state-of-the-art adversarial detection methods, including kernel density (KD) (Feinman et al., 2017), local intrinsic dimensionality (LID) (Ma et al., 2018), mahalanobis distance (MD) (Lee et al., 2018) and LiBRE (Deng et al., 2021). Besides, we construct two new adversarial detection methods based on diffusion models: 1) S-N: using the score norm of raw images, *i.e.*, $\|s_\theta(\mathbf{x}, t)\|^2$. 2) EPS-N: using the norm of the EPS, *i.e.*, $\|S(\mathbf{x})\|^2$. Differently, our proposed EPS-AD further calculates the *maximum mean discrepancy* of EPSs.

Evaluation metric. We evaluate the performance of adversarial detection approaches with the area under the receiver operating characteristic (AUROC), which is a widely used statistic for assessing the discriminatory capacity of distribution models (Jiménez-Valverde, 2012). Considering the computational cost of applying 12 attacks to the classifier, especially for the ImageNet, following Gao et al. (2021), we

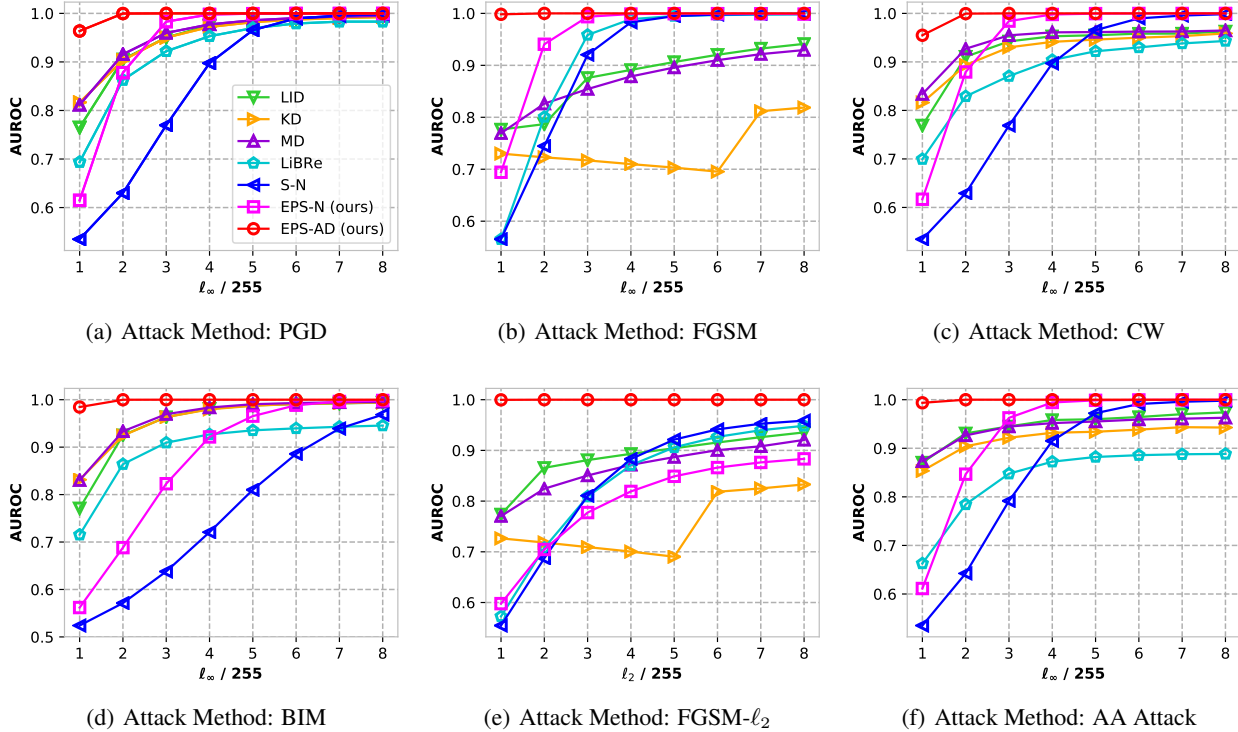


Figure 4. Comparison with adversarial detection methods on ImageNet in terms of AUROC under $\epsilon \in \{1/255, \dots, 8/255\}$ against PGD, FGSM, CW, BIM, FGSM- ℓ_2 , AA. Sub-figures (a) - (f) share the same legend presented in sub-figure (a).

Table 2. Comparison of different adversarial detection methods on ImageNet in terms of AUROC under $\epsilon = 4/255$. The bold number indicates the best results.

AUROC	FGSM	PGD	BIM	CW	FGSM- ℓ_2	BIM- ℓ_2	AA
KD	0.7099	0.9720	0.9797	0.9413	0.7004	0.9775	0.9319
LID	0.8912	0.9750	0.9808	0.9528	0.8932	0.9816	0.9582
MD	0.8786	0.9773	0.9835	0.9609	0.8715	0.9830	0.9518
LiBRe	0.9889	0.9530	0.9269	0.9039	0.8708	0.9211	0.8724
S-N	0.9828	0.8974	0.7208	0.8969	0.8830	0.6762	0.9151
EPS-N (Ours)	0.9987	0.9978	0.9215	0.9978	0.8191	0.7172	0.9943
EPS-AD (Ours)	1.0000	1.0000	1.0000	1.0000	1.0000	1.0000	1.0000

randomly select two disjoint subsets as adversarial and natural samples (each containing 500 samples) and compute the AUROC value over these two subsets. Notably, our method is applicable to different data set sizes, which is verified in Supplementary. Moreover, we set $T^* = 20$ in $S(x)$ on CIFAR-10 and $T^* = 50$ on ImageNet for both our EPS-AD and EPS-N, and set $t^* = 5$ in $s_\theta(\mathbf{x}, t)$ on CIFAR-10 and $t^* = 20$ on ImageNet for S-N.

4.2. Detecting on Known Attacks

We start by comparing EPS-AD with the state-of-the-art adversarial detection methods that are trained with seen adversarial examples, against ℓ_2 and ℓ_∞ threat models. Considering adversarial detection becomes more challenging when the attack intensity of adversarial samples is low, to broadly evaluate the adversarial detection performance, we

compare our method with other baselines on different attacks under different attack intensities. Moreover, to show the best performance of KD, LID and MD, we test the detection performance on corresponding adversarial examples.

Results on CIFAR-10. Figure 3 shows our adversarial detection performance against 6 attacks under different attack intensities $\epsilon \in \{1/255, \dots, 8/255\}$ on CIFAR-10 over WideResNet-28-10 (Zagoruyko & Komodakis, 2016) compared to other baselines. We demonstrate other attacks and more results on WideResNet-70-16 (Gowal et al., 2021) in Supplementary. Obviously, our EPS-AD have much higher AUROC performance than other methods. Critically, we observe that our EPS-AD preserves almost non-degraded AUROC when the attack intensity ϵ surpasses $2/255$ against ℓ_2 and ℓ_∞ attacks, which shows the stability of EPS-AD when detecting challenge adversarial samples.

Table 3. Comparison of AUROC for detecting unseen attacks on CIFAR-10, where “FGSM (seen)” denotes the seen adversarial attack used for the training of KD, LID and MD.

AUROC	FGSM(seen)	PGD	BIM	CW	FGSM- ℓ_2 (seen)	BIM- ℓ_2	AA
KD	0.9213	0.9007	0.9082	0.8339	0.9146	0.9146	0.9135
LID	0.9236	0.8964	0.9028	0.8828	0.9160	0.8984	0.9253
MD	0.9990	0.9855	0.9742	0.9835	0.9992	0.9503	0.9820
S-N	1.0000	0.9998	0.9961	0.9998	0.9885	0.9674	0.9995
EPS-N (Ours)	1.0000	1.0000	0.9996	1.0000	0.9916	0.9883	1.0000
EPS-AD (Ours)	1.0000	1.0000	0.9998	1.0000	0.9995	0.9991	1.0000

Table 4. Comparison of AUROC for detecting transferable attacks on ImageNet, where KD, LID, MD and LiBRe are trained with adversarial examples with ResNet-50 but detect the adversarial examples crafted with ResNet-101.

AUROC	FGSM	PGD	BIM	CW	FGSM- ℓ_2	BIM- ℓ_2	AA
KD	0.7754	0.5999	0.5847	0.7632	0.7906	0.7756	0.7698
LID	0.8467	0.7627	0.7663	0.7704	0.8520	0.7925	0.7967
MD	0.8467	0.7698	0.7684	0.7665	0.8067	0.7759	0.7880
LiBRe	0.9849	0.8414	0.7161	0.8286	0.8489	0.7250	0.8485
S-N	0.9816	0.8965	0.7166	0.8963	0.8764	0.6705	0.9106
EPS-N (Ours)	0.9983	0.9975	0.9178	0.9979	0.8235	0.7215	0.9930
EPS-AD (Ours)	1.0000	1.0000	1.0000	1.0000	1.0000	0.9998	1.0000

In addition, we report quantitative results for adversarial detection under the attack intensity $\epsilon = 4/255$ in Tables 1 and 2. The results show that by employing EPS and measuring their MMD, EPS-AD consistently outperforms existing methods against various attacks in terms of AUROC. We also see that by simply applying the norm of EPS, EPS-N achieves superior adversarial detection performance, which demonstrates the effectiveness of EPS.

Results on ImageNet. We report the adversarial detection performance against ℓ_2 and ℓ_∞ attacks on ImageNet over ResNet-50 (He et al., 2016) in Tables 1, 2 and Figure 4. We defer the results of one widely-used ViT architecture, DeiT-S (Dosovitskiy et al., 2021), in Supplementary. We observe that our approach consistently outperforms baselines under various attacks, especially for detecting PGD, FGSM- ℓ_2 and AA attacks. These results reveal that our proposed EPS-AD is effective even on a large-scale data set. Moreover, we observe that EPS-N exhibits poor results compared to EPS-AD when detecting ℓ_2 attacks (e.g., FGSM- ℓ_2 and BIM- ℓ_2) since the norm of EPS ignores rich information contained in the EPS vector, which is not effective enough to detect on a large-scale data set.

4.3. Detecting on Unseen and Transferable Attacks

In light of poor performance for adversarial detection baselines against unseen attacks and transferable attacks, we evaluate our method in the context of these kinds of attacks.

Detecting on unseen attacks. To detect unseen attacks, we train KD, LID, and MD detectors on CIFAR-10 using only FGSM and FGSM- ℓ_2 adversarial examples and evaluate their performance under other attacks. Combining Tables 3

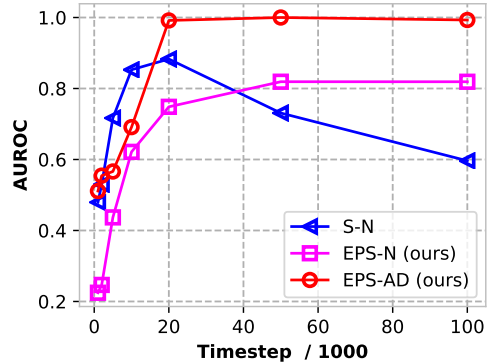


Figure 5. Impact of timestep on ImageNet under different timesteps {1, 2, 5, 10, 20, 50, 100} against FGSM- ℓ_2 .

and 1, 2, we find that adversarial detection performance for MD and LID worsens. An explanation is that their detectors are trained with vectorized features extracted from the seen samples through logistic regression, resulting in their limited generalization on unseen attacks. In contrast, diffusion-based detection methods show superior performance since they directly model the distribution of natural data.

Detecting on transferable attacks. To validate the transferability, we train KD, LID, MD and LiBRe detectors with ResNet-50 but detect the adversarial examples from a surrogate ResNet-101 model. Comparing Tables 4 and 1, 2, the non-diffusion-based methods (e.g., KD, LID, MD and LiBRe) drop significantly against transferable attacks. By contrast, our EPS-AD method achieves significantly better transferability, since it does not rely on specific classifiers, but rather models the distribution of natural data, indicating its versatility in various attack scenarios.

4.4. Ablation Study on Impact of Timestep

We conduct experiments on ImageNet over ResNet-50 to show the effect of the timestep. To this end, we set the total timestep $T = 100$, which is sufficient for both EPS-AD and EPS-N to achieve a good solution. As shown in Figure 5, we draw two observations: 1) our EPS-AD and EPS-N are insensitive to the total timestep T while S-N fluctuates greatly with the timestep t ; 2) As the total timestep T increases, our EPS-AD and EPS-N exhibit progressively better performance, however, this gain gradually decreases when T exceeds the optimal value. This is due to the larger diffusion time, the mean μ_S in Eq. (9) gradually approaches zeros, resulting in a smaller discrepancy between the natural and adversarial distributions. This phenomenon is consistent with the result in Nie et al. (2022) (Theorem 1).

5. Conclusion

In this paper, we propose a new statistic *expected perturbation score* (EPS) to capture the information from multi-view observations of one sample, which is able to distinguish between natural and adversarial data well. Relying on EPS, we propose a novel adversarial detection method, EPS-AD. We provide theoretical analysis to demonstrate the superiority of EPS-AD. Extensive experiments on CIFAR-10 and ImageNet across different network architectures including ResNet, WideResNet and ViT show our EPS-AD successfully detects adversarial samples in various attack scenarios.

Acknowledgements

This work was partially supported by the National Natural Science Foundation of China (NSFC) (62072190, 62122013), Key-Area Research and Development Program Guangdong Province 2018B010107001, Program for Guangdong Introducing Innovative and Entrepreneurial Teams 2017ZT07X183, NSFC Young Scientists Fund No. 62006202, and Guangdong Basic and Applied Basic Research Foundation No. 2022A1515011652.

References

Abdel-Aty, S. Approximate formulae for the percentage points and the probability integral of the non-central χ^2 distribution. *Biometrika*, 41(3/4):538–540, 1954.

Abusnaina, A., Wu, Y., Arora, S., Wang, Y., Wang, F., Yang, H., and Mohaisen, D. Adversarial example detection using latent neighborhood graph. In *Proceedings of the IEEE/CVF International Conference on Computer Vision*, pp. 7687–7696, 2021.

Borgwardt, K. M., Gretton, A., Rasch, M. J., Kriegel, H.-P., Schölkopf, B., and Smola, A. J. Integrating structured biological data by kernel maximum mean discrepancy. *Bioinformatics*, 22(14):e49–e57, 2006.

Carlini, N. and Wagner, D. Towards evaluating the robustness of neural networks. In *2017 IEEE Symposium on Security and Privacy (SP)*, pp. 39–57. IEEE, 2017.

Croce, F. and Hein, M. Reliable evaluation of adversarial robustness with an ensemble of diverse parameter-free attacks. In *Proceedings of the 37th International Conference on Machine Learning*, pp. 2206–2216. PMLR, 2020.

Deng, J., Dong, W., Socher, R., Li, L.-J., Li, K., and Fei-Fei, L. Imagenet: A large-scale hierarchical image database. In *2009 IEEE Conference on Computer Vision and Pattern Recognition*, pp. 248–255. IEEE, 2009.

Deng, Z., Yang, X., Xu, S., Su, H., and Zhu, J. Libre: A practical bayesian approach to adversarial detection. In *Proceedings of the IEEE/CVF Conference on Computer Vision and Pattern Recognition*, pp. 972–982, 2021.

Dhariwal, P. and Nichol, A. Diffusion models beat gans on image synthesis. *Advances in Neural Information Processing Systems*, 34:8780–8794, 2021.

Dong, Y., Liao, F., Pang, T., Su, H., Zhu, J., Hu, X., and Li, J. Boosting adversarial attacks with momentum. In *Proceedings of the IEEE Conference on Computer Vision and Pattern Recognition*, pp. 9185–9193, 2018.

Dong, Y., Pang, T., Su, H., and Zhu, J. Evading defenses to transferable adversarial examples by translation-invariant attacks. In *Proceedings of the IEEE/CVF Conference on Computer Vision and Pattern Recognition*, pp. 4312–4321, 2019.

Dosovitskiy, A., Beyer, L., Kolesnikov, A., Weissenborn, D., Zhai, X., Unterthiner, T., Dehghani, M., Minderer, M., Heigold, G., Gelly, S., et al. An image is worth 16x16 words: Transformers for image recognition at scale. In *International Conference on Learning Representations*, 2021.

Feinman, R., Curtin, R. R., Shintre, S., and Gardner, A. B. Detecting adversarial samples from artifacts. *arXiv preprint arXiv:1703.00410*, 2017.

Gao, R., Liu, F., Zhang, J., Han, B., Liu, T., Niu, G., and Sugiyama, M. Maximum mean discrepancy test is aware of adversarial attacks. In *International Conference on Machine Learning*, pp. 3564–3575. PMLR, 2021.

Gao, R., Wang, J., Zhou, K., Liu, F., Xie, B., Niu, G., Han, B., and Cheng, J. Fast and reliable evaluation of adversarial robustness with minimum-margin attack. In *Proceedings of the 39th International Conference on Machine Learning*, pp. 7144–7163. PMLR, 2022.

- Gong, L.-H., Xiang, L.-Z., Liu, S.-H., and Zhou, N.-R. Born machine model based on matrix product state quantum circuit. *Physica A: Statistical Mechanics and its Applications*, 593:126907, 2022.
- Goodfellow, I. J., Shlens, J., and Szegedy, C. Explaining and harnessing adversarial examples. In *International Conference on Learning Representations*, 2015.
- Gowal, S., Rebuffi, S.-A., Wiles, O., Stimberg, F., Calian, D. A., and Mann, T. A. Improving robustness using generated data. *Advances in Neural Information Processing Systems*, 34:4218–4233, 2021.
- Gretton, A., Borgwardt, K. M., Rasch, M. J., Schölkopf, B., and Smola, A. A kernel two-sample test. *Journal of Machine Learning Research*, 13(1):723–773, 2012.
- Grosse, K., Manoharan, P., Papernot, N., Backes, M., and McDaniel, P. On the (statistical) detection of adversarial examples. *arXiv preprint arXiv:1702.06280*, 2017.
- He, K., Zhang, X., Ren, S., and Sun, J. Deep residual learning for image recognition. In *Proceedings of the IEEE Conference on Computer Vision and Pattern Recognition*, 2016.
- Huang, C.-W., Lim, J. H., and Courville, A. C. A variational perspective on diffusion-based generative models and score matching. *Advances in Neural Information Processing Systems*, 34:22863–22876, 2021.
- Hyvärinen, A. and Dayan, P. Estimation of non-normalized statistical models by score matching. *Journal of Machine Learning Research*, 6(4), 2005.
- Jiménez-Valverde, A. Insights into the area under the receiver operating characteristic curve (auc) as a discrimination measure in species distribution modelling. *Global Ecology and Biogeography*, 21(4):498–507, 2012.
- Jitkrittum, W., Xu, W., Szabó, Z., Fukumizu, K., and Gretton, A. A linear-time kernel goodness-of-fit test. *Advances in Neural Information Processing Systems*, 30, 2017.
- Krizhevsky, A. Learning multiple layers of features from tiny images. (*Technical Report*) *University of Toronto.*, 2009.
- Kurakin, A., Goodfellow, I. J., and Bengio, S. Adversarial examples in the physical world. In *Artificial Intelligence Safety and Security*, pp. 99–112. Chapman and Hall/CRC, 2018.
- Laidlaw, C., Singla, S., and Feizi, S. Perceptual adversarial robustness: Defense against unseen threat models. In *International Conference on Learning Representations*, 2021.
- Lee, K., Lee, K., Lee, H., and Shin, J. A simple unified framework for detecting out-of-distribution samples and adversarial attacks. *Advances in Neural Information Processing Systems*, 31, 2018.
- Li, B. and Vorobeychik, Y. Feature cross-substitution in adversarial classification. *Advances in Neural Information Processing Systems*, 27, 2014.
- Li, J., Zhang, S., Cao, J., and Tan, M. Learning defense transformations for counterattacking adversarial examples. *Neural Networks*, 2023.
- Liu, F., Xu, W., Lu, J., Zhang, G., Gretton, A., and Sutherland, D. J. Learning deep kernels for non-parametric two-sample tests. In *International Conference on Machine Learning*, pp. 6316–6326. PMLR, 2020.
- Long, M., Cao, Y., Wang, J., and Jordan, M. Learning transferable features with deep adaptation networks. In *International Conference on Machine Learning*, pp. 97–105. PMLR, 2015.
- Lu, C., Zhou, Y., Bao, F., Chen, J., Li, C., and Zhu, J. Dpm-solver: A fast ode solver for diffusion probabilistic model sampling in around 10 steps. 2022.
- Ma, X., Li, B., Wang, Y., Erfani, S. M., Wijewickrema, S., Schoenebeck, G., Song, D., Houle, M. E., and Bailey, J. Characterizing adversarial subspaces using local intrinsic dimensionality. In *International Conference on Learning Representations*, 2018.
- Madry, A., Makelov, A., Schmidt, L., Tsipras, D., and Vladu, A. Towards deep learning models resistant to adversarial attacks. In *International Conference on Learning Representations*, 2018.
- Nie, W., Guo, B., Huang, Y., Xiao, C., Vahdat, A., and Anandkumar, A. Diffusion models for adversarial purification. In *International Conference on Machine Learning*, 2022.
- Niu, S., Wu, J., Zhang, Y., Chen, Y., Zheng, S., Zhao, P., and Tan, M. Efficient test-time model adaptation without forgetting. In *International conference on machine learning*, pp. 16888–16905. PMLR, 2022.
- Niu, S., Wu, J., Zhang, Y., Wen, Z., Chen, Y., Zhao, P., and Tan, M. Towards stable test-time adaptation in dynamic wild world. In *The Eleventh International Conference on Learning Representations*, 2023.
- Ozbulak, U., Van Messeem, A., and De Neve, W. Impact of adversarial examples on deep learning models for biomedical image segmentation. In *MICCAI*, 2019.

- Pang, T., Zhang, H., He, D., Dong, Y., Su, H., Chen, W., Zhu, J., and Liu, T.-Y. Two coupled rejection metrics can tell adversarial examples apart. In *Proceedings of the IEEE/CVF Conference on Computer Vision and Pattern Recognition*, pp. 15223–15233, 2022.
- Radford, A., Metz, L., and Chintala, S. Unsupervised representation learning with deep convolutional generative adversarial networks. In *International Conference on Learning Representations*, 2016.
- Raghuram, J., Chandrasekaran, V., Jha, S., and Banerjee, S. A general framework for detecting anomalous inputs to dnn classifiers. In *International Conference on Machine Learning*, pp. 8764–8775. PMLR, 2021.
- Ramesh, A., Dhariwal, P., Nichol, A., Chu, C., and Chen, M. Hierarchical text-conditional image generation with clip latents. *arXiv preprint arXiv:2204.06125*, 2022.
- Rombach, R., Blattmann, A., Lorenz, D., Esser, P., and Ommer, B. High-resolution image synthesis with latent diffusion models. In *Proceedings of the IEEE/CVF Conference on Computer Vision and Pattern Recognition*, pp. 10684–10695, 2022.
- Saharia, C., Chan, W., Saxena, S., Li, L., Whang, J., Denton, E., Ghasemipour, S. K. S., Ayan, B. K., Mahdavi, S. S., Lopes, R. G., et al. Photorealistic text-to-image diffusion models with deep language understanding. *arXiv preprint arXiv:2205.11487*, 2022.
- Shi, C., Holtz, C., and Mishne, G. Online adversarial purification based on self-supervision. In *International Conference on Learning Representations*, 2021.
- Song, Y. and Ermon, S. Generative modeling by estimating gradients of the data distribution. *Advances in Neural Information Processing Systems*, 32, 2019.
- Song, Y., Sohl-Dickstein, J., Kingma, D. P., Kumar, A., Ermon, S., and Poole, B. Score-based generative modeling through stochastic differential equations. In *International Conference on Learning Representations*, 2021.
- Stutz, D., Hein, M., and Schiele, B. Confidence-calibrated adversarial training: Generalizing to unseen attacks. In *International Conference on Machine Learning*, pp. 9155–9166. PMLR, 2020.
- Szegedy, C., Zaremba, W., Sutskever, I., Bruna, J., Erhan, D., Goodfellow, I., and Fergus, R. Intriguing properties of neural networks. In *International Conference on Learning Representations*, 2014.
- Vincent, P. A connection between score matching and denoising autoencoders. *Neural Computation*, 23(7):1661–1674, 2011.
- Wang, X. and He, K. Enhancing the transferability of adversarial attacks through variance tuning. In *Proceedings of the IEEE/CVF Conference on Computer Vision and Pattern Recognition*, pp. 1924–1933, 2021.
- Wong, E., Rice, L., and Kolter, J. Z. Fast is better than free: Revisiting adversarial training. In *International Conference on Learning Representations*, 2020.
- Xie, C., Zhang, Z., Zhou, Y., Bai, S., Wang, J., Ren, Z., and Yuille, A. L. Improving transferability of adversarial examples with input diversity. In *Proceedings of the IEEE/CVF Conference on Computer Vision and Pattern Recognition*, pp. 2730–2739, 2019.
- Yoon, J., Hwang, S. J., and Lee, J. Adversarial purification with score-based generative models. In *International Conference on Machine Learning*, pp. 12062–12072. PMLR, 2021.
- Zagoruyko, S. and Komodakis, N. Wide residual networks. In *British Machine Vision Conference 2016*, 2016.
- Zhang, J., Wu, W., Huang, J.-t., Huang, Y., Wang, W., Su, Y., and Lyu, M. R. Improving adversarial transferability via neuron attribution-based attacks. In *Proceedings of the IEEE/CVF Conference on Computer Vision and Pattern Recognition*, pp. 14993–15002, 2022.
- Zhu, Y., Zhuang, F., and Wang, D. Aligning domain-specific distribution and classifier for cross-domain classification from multiple sources. In *Proceedings of the AAAI Conference on Artificial Intelligence*, volume 33, pp. 5989–5996, 2019.

Supplementary Materials for “Detecting Adversarial Data by Probing Multiple Perturbations Using Expected Perturbation Score”

In Supplementary, we provide detailed proofs of the theorem and corollary, descriptions of related works, more details and more experimental results of the proposed EPS-AD. We organize the supplementary into the following sections. In Section A, we provide descriptions of related works regarding adversarial detection. In Section B, we derive the proofs of the theorem and corollary. In Section C, we demonstrate the pseudo-code of our proposed EPS-AD. In Section D, we present detailed implementation of our experiments. In Section E, we show the impact of EPS in our method. In Section F, we study the impact of adding perturbations over samples in our method. In Section G, we report more comparison results, more ablation studies of our proposed EPS-AD.

A. Related Work

Diffusion models. Diffusion models have emerged as a powerful generative model in many synthesis tasks (Song & Ermon, 2019; Dhariwal & Nichol, 2021; Saharia et al., 2022; Rombach et al., 2022; Ramesh et al., 2022). Since then, many researchers exploit the diffusion model to adversarial purification for improving the robustness of model (Nie et al., 2022; Yoon et al., 2021), where the score becomes a powerful means. Yet, only few researchers apply them to adversarial detection. Recently, Yoon et al. (2021) employ the score model to purify the adversarial examples and use the norm of scores as the stopping condition of the purification. They also demonstrate some results about the norm of score in distinguishing adversarial samples from natural samples. However, this criterion is not effective enough for adversarial detection. In our work, we comprehensively consider multiple scores of perturbed samples, where these perturbed samples are from the same sample, and exploit rich information from these scores for adversarial detection. We empirically compare our approach to these methods and find that our approach outperforms these methods by a large margin.

Adversarial attack. Numerous studies have been proposed to attack neural networks by slightly modifying the input data to trigger misclassifications of classifiers. We enumerate a series of such works in what follows. Fast Gradient Sign Method (FGSM) (Goodfellow et al., 2015) simply adds small noise along the gradient of the loss function. To further adjust the direction of increment, Kurakin et al. (2018) propose Basic Iterative Method (BIM) that extends FGSM to iteratively take multiple steps. Madry et al. (2018) propose Projected Gradient Descent (PGD) by combining the iterative method with random initialization for the adversarial example. Meanwhile, Dong et al. (2018) propose Momentum Iterative Method (MIM) by adding a momentum term to BIM for achieving a more stable attack. Besides, Dong et al. (2019) propose Translation-Invariant Method (TIM) by optimizing the perturbation over translated images to obtain more transferable attacks, which can be incorporated into the methods FGSM and BIM. To further improve the transferability of attack, Wang & He (2021) propose variance tuning to guide the gradient update, namely VMI-FGSM; Zhang et al. (2022) conduct feature-level attacks with more accurate neuron importance estimations, called Neuron Attribution-based (NAA) attack. Besides the non-targeted attack methods mentioned above, there are also many methods that perturb data to one target label. For example, Carlini & Wagner (2017) perform an attack by incorporating the iterative mechanism of BIM, called CW. Besides, there are approaches that combine multiple attacks, such as the AutoAttack (Croce & Hein, 2020) and the Minimum-margin (MM) attack (Gao et al., 2022), the faster version of AutoAttack. The various attacks may cause serious consequences in security-critical tasks, raising an urgent requirement for advanced techniques to achieve a robust model.

Adversarial detection. To ensure the safety of machine learning system, a plethora of exploration for adversarial detection has attracted increasing sight. The most common idea is to filter out adversarial samples from test data using a trained binary classifier. Recently, statistics on hidden-layer features of DNNs are widely considered for adversarial detection. Feinman et al. (2017) train a logistic regression classifier using Kernel Density (KD) of features in the last hidden layer, as well as Bayesian Uncertainty (BU) as a basis. Ma et al. (2018) consider the local intrinsic dimensionality (LID) of the features of DNNs as the characteristics for detection. Lee et al. (2018) use a mahalanobis distance-based score to detect adversarial examples. Raghuram et al. (2021) extract the intermediate layer representations of DNNs in the form of a meta-algorithm

with configurable components for detection. In addition, [Deng et al. \(2021\)](#) train a Bayesian neural network by adding uniform noises to the samples. Another mainstream strategy for handling adversarial examples is to equip the classifier with a rejection option. [Stutz et al. \(2020\)](#) propose a confidence-calibrated adversarial training framework by inducing the model towards low confidence predictions on adversarial examples to decide which sample to reject. [Pang et al. \(2022\)](#) suggest coupling confidence with a proposed R-Con as metrics to separate adversarial samples from normal ones. However, these methods train a tailored detector for some specific attacks or for a specific classifier, which largely overlooks the modeling for data distribution, leading to their limited performance under unknown attacks.

B. Proofs in Section 3

B.1. Proof of Theorem 1

Theorem 1 *Assuming that the distribution of natural data $p(\mathbf{x}) = \mathcal{N}(\boldsymbol{\mu}_x, \sigma_x^2 \mathbf{I})$, where \mathbf{I} is an identity matrix, given a perturbation transition kernel $p_{0t}(\mathbf{x}_t | \mathbf{x}_0) = \mathcal{N}(\gamma_t \mathbf{x}_0, \sigma_t^2 \mathbf{I})$ with γ_t and σ_t being the time-dependent noise schedule, then the following three conclusions hold:*

- 1) For $\forall \mathbf{x} \sim p(\mathbf{x})$, $S(\mathbf{x}) \sim \mathcal{N}(\mathbf{0}, \sigma_S^2 \mathbf{I})$;
- 2) For $\forall \mathbf{y} \sim p(\mathbf{x})$ and adversarial sample $\hat{\mathbf{y}} = \mathbf{y} + \boldsymbol{\varepsilon}$, $S(\hat{\mathbf{y}}) \sim \mathcal{N}(-\boldsymbol{\mu}_S, \sigma_S^2 \mathbf{I})$;
- 3) For $\forall \mathbf{x}, \mathbf{y} \sim p(\mathbf{x})$ and adversarial sample $\hat{\mathbf{y}} = \mathbf{y} + \boldsymbol{\varepsilon}$,

$$S(\mathbf{x}) - S(\mathbf{y}) \sim \mathcal{N}(\mathbf{0}, 2\sigma_S^2 \mathbf{I}); \quad (12)$$

$$S(\mathbf{x}) - S(\hat{\mathbf{y}}) \sim \mathcal{N}(\boldsymbol{\mu}_S, 2\sigma_S^2 \mathbf{I}), \quad (13)$$

where $\boldsymbol{\mu}_S = \mathbb{E}_t \frac{\boldsymbol{\varepsilon}}{\gamma_t^2 \sigma_x^2 + \sigma_t^2}$ and $\sigma_S^2 = \mathbb{E}_t \frac{1}{\gamma_t^2 \sigma_x^2 + \sigma_t^2}$.

Proof. 1) Based on the distribution $p(\mathbf{x})$, i.e., $\mathbf{x}_0 = \mathbf{x} \sim \mathcal{N}(\boldsymbol{\mu}_x, \sigma_x^2 \mathbf{I})$, we obtain $\mathbf{x}_0 = \boldsymbol{\mu}_x + \sigma_x \mathbf{z}$ with $\mathbf{z} \sim \mathcal{N}(\mathbf{0}, \mathbf{I})$; based on the perturbation transition kernel $p_{0t}(\mathbf{x}_t | \mathbf{x}_0) = \mathcal{N}(\gamma_t \mathbf{x}_0, \sigma_t^2 \mathbf{I})$, we have $\mathbf{x}_t = \gamma_t \mathbf{x}_0 + \sigma_t \mathbf{z}$. Combining the distribution of \mathbf{x} and \mathbf{x}_0 , we have

$$\mathbf{x}_t = \gamma_t \boldsymbol{\mu}_x + \sqrt{\gamma_t^2 \sigma_x^2 + \sigma_t^2} \mathbf{z}, \quad \text{i.e., } \mathbf{x}_t \sim \mathcal{N}(\gamma_t \boldsymbol{\mu}_x, \gamma_t^2 \sigma_x^2 + \sigma_t^2) \quad (14)$$

For $\mathbf{x}_t \sim p_t(\mathbf{x}) = \mathcal{N}(\gamma_t \boldsymbol{\mu}_x, \gamma_t^2 \sigma_x^2 + \sigma_t^2)$, we calculate the derivation

$$\nabla_{\mathbf{x}} \log p_t(\mathbf{x}) = -\frac{\mathbf{x}_t - \gamma_t \boldsymbol{\mu}_x}{\gamma_t^2 \sigma_x^2 + \sigma_t^2} = -\frac{1}{\sqrt{\gamma_t^2 \sigma_x^2 + \sigma_t^2}} \mathcal{N}(\mathbf{0}, \mathbf{I}). \quad (15)$$

Taking expectation to t , we give the distribution of $S(\mathbf{x})$

$$S(\mathbf{x}) \sim \mathcal{N}(\mathbf{0}, \sigma_S^2 \mathbf{I}), \quad \text{where } \sigma_S^2 = \mathbb{E}_t \frac{1}{\gamma_t^2 \sigma_x^2 + \sigma_t^2}. \quad (16)$$

2) Based on $\mathbf{y} \sim p(\mathbf{x})$ and $\hat{\mathbf{y}} = \mathbf{y} + \boldsymbol{\varepsilon}$, we obtain $\hat{\mathbf{y}}_0 = \hat{\mathbf{y}} \sim \mathcal{N}(\boldsymbol{\mu}_x + \boldsymbol{\varepsilon}, \sigma_x^2 \mathbf{I})$. Then, we have

$$\nabla_{\hat{\mathbf{y}}} \log p_t(\hat{\mathbf{y}}) = -\frac{\mathbf{y}_t + \boldsymbol{\varepsilon} - \gamma_t \boldsymbol{\mu}_x}{\gamma_t^2 \sigma_x^2 + \sigma_t^2} = -\frac{1}{\sqrt{\gamma_t^2 \sigma_x^2 + \sigma_t^2}} \mathcal{N}(\mathbf{0}, \mathbf{I}) - \frac{\boldsymbol{\varepsilon}}{\gamma_t^2 \sigma_x^2 + \sigma_t^2}, \quad (17)$$

where the last equation is based on $p_t(\mathbf{y}) = p_t(\mathbf{x}) = \mathcal{N}(\gamma_t \boldsymbol{\mu}_x, \gamma_t^2 \sigma_x^2 + \sigma_t^2)$.

Taking expectation to t , we give the distribution of $S(\hat{\mathbf{y}})$

$$S(\hat{\mathbf{y}}) \sim \mathcal{N}(-\boldsymbol{\mu}_S, \sigma_S^2 \mathbf{I}), \quad \text{where } \boldsymbol{\mu}_S = \mathbb{E}_t \frac{\boldsymbol{\varepsilon}}{\gamma_t^2 \sigma_x^2 + \sigma_t^2} \quad \text{and} \quad \sigma_S^2 = \mathbb{E}_t \frac{1}{\gamma_t^2 \sigma_x^2 + \sigma_t^2}. \quad (18)$$

3) According to the additive property of the Gaussian distribution, combining Eq. (16) and Eq. (18), we obtain the third conclusion. □

B.2. Proof of Corollary 1

Corollary 1 Considering the Gaussian kernel $k(\mathbf{a}, \mathbf{b}) = \exp\left(-\|\mathbf{a} - \mathbf{b}\|^2 / (2\sigma^2)\right)$ and the assumption in Theorem 1, for $\forall 0 < \eta < 1$, the probability of $P\{k(S(\mathbf{x}), S(\hat{\mathbf{y}})) > \eta\}$ is given by

$$P\{k(S(\mathbf{x}), S(\hat{\mathbf{y}})) > \eta\} = \int_0^C \chi_d^2(z) dz, \quad (19)$$

where $z = \|\boldsymbol{\mu}_S\|^2$ with $\boldsymbol{\mu}_S$ being the mean of $S(\mathbf{x}) - S(\hat{\mathbf{y}})$, C is a constant for given η and σ , χ^2 is the probability density function of noncentral chi-squared distribution with d degrees of freedom (Abdel-Aty, 1954).

Proof. Based on the Gaussian kernel $k(\mathbf{a}, \mathbf{b})$, we have

$$P\{\kappa(S(\mathbf{x}), S(\hat{\mathbf{y}})) > \eta\} = P\left\{\exp\left(-\|S(\mathbf{x}) - S(\hat{\mathbf{y}})\|^2 / (2\sigma^2)\right) > \eta\right\} = P\left\{\|S(\mathbf{x}) - S(\hat{\mathbf{y}})\|^2 < -2\sigma^2 \ln \eta\right\}. \quad (20)$$

Let $\boldsymbol{\xi} \sim S(\mathbf{x}) - S(\hat{\mathbf{y}})$, then $\boldsymbol{\xi}_i \sim \mathcal{N}((\boldsymbol{\mu}_S)_i, 2\sigma_S^2)$, thus we have

$$P\{\kappa(S(\mathbf{x}), S(\hat{\mathbf{y}})) > \eta\} = P\left\{\sum_{i=1}^d \boldsymbol{\xi}_i^2 < -2\sigma^2 \ln \eta\right\} = P\left\{\sum_{i=1}^d \left(\frac{\boldsymbol{\xi}_i}{\sqrt{2}\sigma_S}\right)^2 < \frac{-\sigma^2 \ln \eta}{\sigma_S^2}\right\} \quad (21)$$

Note that $\frac{\boldsymbol{\xi}_i}{\sqrt{2}\sigma_S} \sim \mathcal{N}((\boldsymbol{\mu}_S)_i, 1)$, based on the definition of noncentral chi-squared distribution (Abdel-Aty, 1954), we have

$$\sum_{i=1}^d \left(\frac{\boldsymbol{\xi}_i}{\sqrt{2}\sigma_S}\right)^2 \sim \chi_d^2(\|\boldsymbol{\mu}_S\|^2) \quad (22)$$

Let $C = \frac{-\sigma^2 \ln \eta}{\sigma_S^2}$ and $z = \|\boldsymbol{\mu}_S\|^2$, we obtain the conclusion

$$P\{k(\mathbf{x}, \hat{\mathbf{y}}) > \eta\} = \int_0^C \chi_d^2(z) dz. \quad (23)$$

□

C. Pseudo-code of EPS-AD

Algorithm 1 Expected Perturbation Score for Adversarial Detection (EPS-AD).

input A natural sample set $\{\mathbf{x}_0^{(i)}\}_{i=1}^n$, a test sample $\tilde{\mathbf{x}}_0$, a pre-trained score model $s_\theta(\mathbf{x}_t, t)$ and a diffusion timestep T^* .

output MMD between EPS of the test sample $\tilde{\mathbf{x}}_0$ and EPSs of natural samples $\{\mathbf{x}_0^{(i)}\}$.

- 1: Set initial time step $t = 1$;
 - 2: **for** $t = 1, \dots, T^*$ **do**
 - 3: Obtain perturbed natural samples $\{\mathbf{x}_t^{(i)}\}_{i=1}^n$ according to $p_{0t}(\mathbf{x}_t | \mathbf{x}_0)$.
 - 4: Obtain perturbed test sample $\tilde{\mathbf{x}}_t^{(i)}$ according to $p_{0t}(\tilde{\mathbf{x}}_t | \tilde{\mathbf{x}}_0)$.
 - 5: **end for**
 - 6: Compute EPSs of natural samples $\{S(\mathbf{x}^{(i)})\}_{i=1}^n$ using Eq. (7).
 - 7: Compute EPS of the test sample $S(\tilde{\mathbf{x}})$ using Eq. (7).
 - 8: Compute the deep kernel MMD between $\{S(\mathbf{x}^{(i)})\}_{i=1}^n$ and $S(\tilde{\mathbf{x}})$ using Eq. (10).
-

D. More Details for Experiment Settings

D.1. Implementation Details of Our Method

Our adversarial detection method is built upon diffusion models. Specifically, we consider the pre-trained diffusion model of Score SDE for CIFAR-10 following Song et al. (2021) and choose the `vp/cifar10_ddpmpp_deep_continuous` checkpoint from the `score_sde` library¹; for ImageNet, we consider the pre-trained diffusion model of Guided Diffusion following Dhariwal & Nichol (2021) and use the `256 × 256_diffusion (unconditional)` checkpoint from the `guided-diffusion` library².

For classifiers, we use pre-trained WiderResNet-28-10 (Zagoruyko & Komodakis, 2016) and WiderResNet-70-16 (Gowal et al., 2021) for CIFAR-10, and ResNet-50, ResNet-101 (He et al., 2016), and DeiT-S (Dosovitskiy et al., 2021) for ImageNet. For attacks, we consider 8 attack intensities $\epsilon \in \{1/255, \dots, 8/255\}$ with iterative attacks run for 5 steps using step size $\epsilon/5$ under 12 different ℓ_2 and ℓ_∞ attack methods to generate adversarial examples, including PGD, PGD- ℓ_2 (Madry et al., 2018), FGSM, FGSM- ℓ_2 (Goodfellow et al., 2015), BIM, BIM- ℓ_2 (Kurakin et al., 2018), MIM (Dong et al., 2018), TIM (Dong et al., 2019), CW (Carlini & Wagner, 2017), DLMIM (Xie et al., 2019) and two adaptive attacks AutoAttack (AA) (Croce & Hein, 2020) and Minimum-Margin Attack (MM) (Gao et al., 2022) that is a faster version of AA. For evaluation, we choose the area under the receiver operating characteristic curve (AUROC) as metric for adversarial detection.

In our proposed EPS-AD, we employ the deep kernel MMD algorithm as described by Liu et al. (2020). The deep kernel is defined as $k_\omega(S(\mathbf{x}), S(\mathbf{y})) = [(1 - \epsilon_0)\kappa(\phi_\omega(S(\mathbf{x})), \phi_\omega(S(\mathbf{y}))) + \epsilon_0]q(S(\mathbf{x}), S(\mathbf{y}))$, where $\epsilon_0 \in (0, 1)$, ϕ_ω is a deep neural network, κ is a Gaussian kernel with bandwidth σ_{ϕ_ω} and $q(S(\mathbf{x}), S(\mathbf{y}))$ is a Gaussian kernel with bandwidth σ_q . We use the deep network ϕ_ω based on the discriminator architecture in DCGAN (Radford et al., 2016). Through all our experiments, we use only FGSM and FGSM- ℓ_2 adversarial samples ($\epsilon = 1/255$), 10,000 each, along with 10,000 nature samples to calculate their EPSs and train the parameters $\{\epsilon_0, \phi_\omega, \sigma_{\phi_\omega}, \sigma_q\}$ to detect all the other types of attacks with 8 varying attack intensities following Algorithm 1 in Liu et al. (2020)³, in which we set the learning rate to 0.00002 for CIFAR-10 and 0.002 for ImageNet. The deep kernel can also be trained on a general public dataset which we leave for our future work. Note that our method is suitable for detecting all the ℓ_2 and ℓ_∞ adversarial samples. We conduct our experiments based on Python 3.7 and Pytorch 1.7.1 on a server with 1× RTX 3090 GPU.

D.2. Implementation Details of Baselines

We choose three standard adversarial detection approaches, KD (Feinman et al., 2017), LID (Ma et al., 2018) and MD (Lee et al., 2018) as baselines for both CIFAR-10 and ImageNet, as well as LiBre (Deng et al., 2021) individually on the ImageNet, which trains a Bayesian neural network by adding the uniform noises into the samples.

KD & LID & MD. We implement KD following the codebase⁴, LID following the codebase⁵, and MD following the codebase⁶. These three methods train a logistic regressor to distinguish natural, noisy and adversarial samples. To show their best performance for adversarial detection, we choose the noise scale of the ℓ_2 distance in KD, LID and MD as 40, 1, 10 on CIFAR-10 and 20, 1, 10 on ImageNet. Besides, for KD, we choose bandwidth as 10 on CIFAR-10 and 20 on ImageNet.

LiBre. We implement LiBre on ImageNet following their codebase⁷. We evaluate its performance on ResNet-50 and ResNet-101 to make a comparison.

D.3. Implementation Details of Figure 1

For the results in Figure 1, we calculate the norms of scores of natural samples and adversarial samples at different purification timesteps using a score model pre-trained on ImageNet, where these adversarial samples are crafted by FGSM with $\epsilon = 1/255$. Before feeding these samples into the score model, we do not perturb them again. To better demonstrate these results, we normalize score norm with the maximum of scores in each timestep.

¹https://github.com/yang-song/score_sde

²<https://github.com/openai/guided-diffusion>

³<https://github.com/fengliu90/DK-for-TST>

⁴<https://github.com/rfeinman/detecting-adversarial-samples>

⁵https://github.com/xingjunm/lid_adversarial_subspace_detection

⁶https://github.com/pokaxpoka/deep_Mahalanobis_detector

⁷<https://github.com/thudzj/ScalableBDL>

E. Impact of EPS for EPS-AD

In our method EPS-AD, we use diffusion-based score model to calculate the characteristics of samples, *i.e.*, EPS, which has the same dimension as this sample. In this experiment, we investigate the impact of EPS in our method. As a result, we remove the calculation of EPS from our method, instead using the raw sample as their characteristic. Table 5 shows adversarial detection performance of our method against 6 attacks under attack intensities $\epsilon \in \{2/255, 4/255\}$ on ImageNet over ResNet-50 compared to that without EPS. Obviously, EPS-AD without employing EPS demonstrates significant performance drop ($\approx 28\%$ ↓), suggesting the superiority of our proposed EPS in distinguishing between adversarial and natural samples.

Table 5. Impact of EPS with ResNet-50 on ImageNet under $\epsilon = 2/255$ and $\epsilon = 4/255$.

Perturbation	Method	FGSM	PGD	BIM	MIM	TIM	CW
$\epsilon = 2/255$	EPS-AD (w/o EPS)	0.7132	0.7108	0.7101	0.7119	0.7120	0.7107
	EPS-AD (w/ EPS)	1.0000	0.9997	0.9999	1.0000	0.9983	0.9995
$\epsilon = 4/255$	EPS-AD (w/o EPS)	0.7176	0.7144	0.7131	0.7156	0.7156	0.7142
	EPS-AD (w/ EPS)	1.0000	1.0000	1.0000	1.0000	1.0000	1.0000
Perturbation	Method	DI_MIM	PGD- ℓ_2	FGSM- ℓ_2	BIM- ℓ_2	MM	AA
$\epsilon = 2/255$	EPS-AD (w/o EPS)	0.7117	0.7118	0.7133	0.7097	0.7066	0.7067
	EPS-AD (w/ EPS)	0.9999	1.0000	1.0000	0.9999	1.0000	1.0000
$\epsilon = 4/255$	EPS-AD (w/o EPS)	0.7156	0.7154	0.7175	0.7128	0.7101	0.7104
	EPS-AD (w/ EPS)	1.0000	1.0000	1.0000	1.0000	1.0000	1.0000

F. Impact of Adding Perturbations over Samples for EPS-AD

Adding perturbations into the samples is critical for our proposed EPS-AD. To investigate the impact of this operation, we conduct ablation studies against 6 adversarial attack methods on ImageNet. Table 6 demonstrates adversarial detection performance of EPS-AD against 6 attacks under $\epsilon = 1/255$ on ImageNet over ResNet-50 compared to that without adding perturbations. We observe that the adversarial detection performance is significantly improved with adding perturbations. Specifically, our method obtains about 1.86% ↑ on average of 12 attacks, in which the maximum is 4.84% ↑ against BIM- ℓ_2 . This coincides with the conclusion in Theorem 1 that adding the perturbations helps distinguish between adversarial and natural samples.

Table 6. Impact of adding perturbations with ResNet-50 on ImageNet under $\epsilon = 1/255$.

Method	PGD	BIM	CW	FGSM- ℓ_2	BIM- ℓ_2	AA
EPS-AD (w/o perturbation)	0.9274	0.9405	0.9257	0.9960	0.9443	0.9835
EPS-AD (w/ perturbation)	0.9637	0.9845	0.9549	0.9997	0.9927	0.9936
Method	FGSM	MIM	TIM	DI_MIM	PGD- ℓ_2	MM
EPS-AD (w/o perturbation)	0.9954	0.9885	0.9397	0.9791	0.9858	0.9818
EPS-AD (w/ perturbation)	0.9982	0.9972	0.9561	0.9817	0.9961	0.9928

G. More Results of Adversarial Detection

To further evaluate the effectiveness of our proposed EPS-AD, in subsection G.1, we conduct more comparison experiments on detecting more adversarial attacks on ImageNet and CIFAR-10 datasets. To demonstrate the generalization of EPS-AD, we conduct more experiments on detecting unseen attacks and transferable attacks. In subsection G.2, we additionally study the mechanism of EPS-AD by demonstrating the impact of time steps, set size, low attack intensity, transferability across datasets, robustness against adaptive attacks and inference efficiency. We provide extra results of all compared experiments in Tables 7, 8, 9 and Figures 6, 7, 8, as supplements of additional attack methods corresponding to the main body.

G.1. More Comparison Experiments

More comparison results on basic setup. In Table 7, we provide additional attack results including MIM, TIM, DI_MIM, PGD- ℓ_2 , MM on CIFAR-10 and ImageNet. We observe that EPS-AD keeps dominant position under these attacks, EPS-N and S-N exhibit poor performance on ImageNet due to the fact that these two methods use the norm of vectors and thus overlook the rich information that can be deviated from the vector. Moreover, we find that in Figure 6 and Figure 7, most adversarial detection methods suffer from the extremely low attack intensity (e.g., $\epsilon = 1/255$). In contrast, our method EPS-AD still has promising detection performance (refer to Table 21 for more quantitative results).

Table 7. More results of different adversarial detection methods on CIFAR-10 and ImageNet in terms of AUROC under $\epsilon = 4/255$ (MIM, TIM, DI, MIM, PGD- ℓ_2 , MM).

Dataset	Method	MIM	TIM	DI_MIM	PGD- ℓ_2	MM
CIFAR-10	KD	0.8863	0.8856	0.8459	0.9296	0.9116
	LID	0.9135	0.8781	0.8638	0.9426	0.9380
	MD	0.9890	0.9998	0.9846	0.9958	0.9836
	S-N	0.9993	0.9985	0.9980	1.0000	0.9994
	EPS-N (Ours)	0.9999	0.9996	0.9996	1.0000	0.9996
	EPS-AD (Ours)	1.0000	0.9993	0.9999	1.0000	0.9995
ImageNet	KD	0.9669	0.9317	0.7402	0.9809	0.9377
	LID	0.9665	0.9397	0.7658	0.9833	0.9575
	MD	0.9664	0.9365	0.8612	0.9858	0.9585
	LiBRe	0.9483	0.8772	0.9968	0.9532	0.8697
	S-N	0.9087	0.8310	0.9143	0.9505	0.9090
	EPS-N (Ours)	0.9778	0.9114	0.9779	0.9989	0.9939
EPS-AD (Ours)	1.0000	1.0000	1.0000	1.0000	1.0000	

More comparison results on unseen and transferable attacks. We also compare our EPS-AD with KD, LID MD and LiBRe under 6 additional unseen or transferable attacks (MIM, TIM, DI_MIM, PGD- ℓ_2 , MM, VMI-FGSM (Wang & He, 2021)) to further evaluate the effectiveness of our method. In Table 8 and Table 9, Our approach consistently exhibits superior generalization compared to other baselines.

Table 8. More results of AUROC for detecting the unseen attacks (MIM, TIM, DI_MIM, PGD- ℓ_2 , MM) on CIFAR-10. “FGSM (seen)” denotes the seen adversarial attack used for the training of KD, LID and MD.

Method	FGSM(seen)	MIM	TIM	DI_MIM	PGD- ℓ_2	MM
KD	0.9213	0.8867	0.8876	0.8549	0.9303	0.9114
LID	0.9236	0.9131	0.8479	0.8631	0.9090	0.9244
MD	0.9990	0.9858	0.9998	0.9791	0.9958	0.9829
S-N	1.0000	0.9993	0.9985	0.9980	1.0000	0.9994
EPS-N (Ours)	1.0000	0.9999	0.9996	0.9996	1.0000	0.9996
EPS-AD (Ours)	1.0000	1.0000	0.9993	0.9999	1.0000	0.9995

More comparison results on CIFAR-10 over robust WideResNet-70-16. We further compare our method with baselines on an adversarial trained classifier on CIFAR-10, e.g., WideResNet-70-16 (Gowal et al., 2021) against various attacks. In Tables 10, 11, We observe that diffusion-based detection methods are much better than other baselines trained with specific

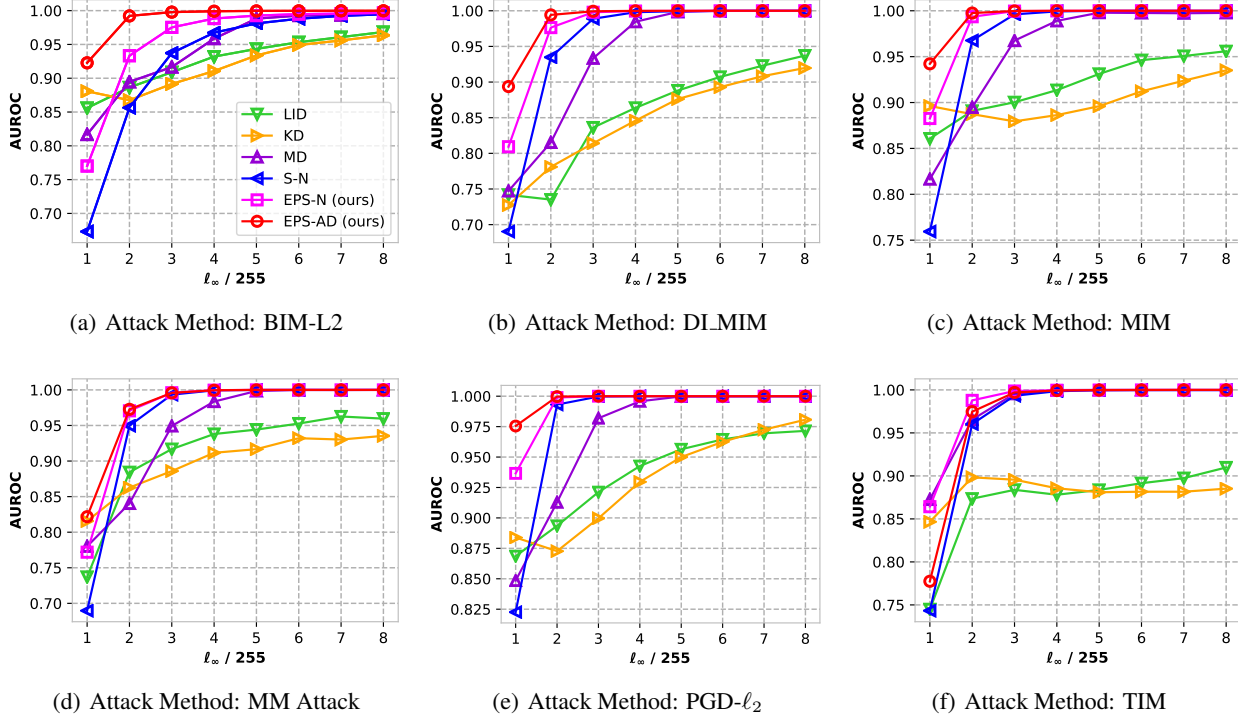


Figure 6. More Results of adversarial detection on CIFAR-10. Sub-figures (a) - (f) report the AUROC on different attacks under $\epsilon \in \{1/255, \dots, 8/255\}$ and share the same legend in sub-figure (a).

Table 9. More results of AUROC for detecting the transferable attacks (MIM, TIM, DL_MIM, PGD- ℓ_2 , MM, VMI-FGSM) on ImageNet, where KD, LID, MD and LiBRe are trained with adversarial examples with ResNet-50 but detect the adversarial examples crafted with ResNet-101.

Method	MIM	TIM	DL_MIM	PGD- ℓ_2	MM	VMI-FGSM
KD	0.6355	0.7006	0.7558	0.7028	0.7381	0.7669
LID	0.7780	0.7978	0.7654	0.7734	0.7913	0.7386
MD	0.7756	0.7612	0.8395	0.7827	0.7864	0.8039
LiBRe	0.8966	0.7317	0.9722	0.8749	0.8388	0.9944
S-N	0.9049	0.8216	0.9117	0.9490	0.9043	0.8638
EPS-N (Ours)	0.9771	0.9049	0.9765	0.9987	0.9930	0.9609
EPS-AD (Ours)	1.0000	1.0000	1.0000	1.0000	1.0000	1.0000

adversarial samples. One possible reason is that adversarial samples are difficult to deceive robust classifiers, which means that such adversarial samples are ineffective for training effective detectors.

More comparison results on ImageNet over DeiT-S. We further make an attempt on Vision-transformer-based architecture (*i.e.* DeiT-S (Dosovitskiy et al., 2021)) on ImageNet. Considering the specificity of the vision-transformer-based structure, we compare our method to three baselines (LID, S-N and EPS-N). From Table 12, our method exhibits consistent superiority when compared to other baselines, suggesting the versatility of EPS-AD with different architectures.

More comparison results with rejection option method. We further compare our method with R-Rejection (Pang et al., 2022) against FGSM attack ($\epsilon = 4/255$) on CIFAR-10. From Table 13, we find that our method EPS-AD outperforms the baseline by a large margin, demonstrating the superiority of our method.

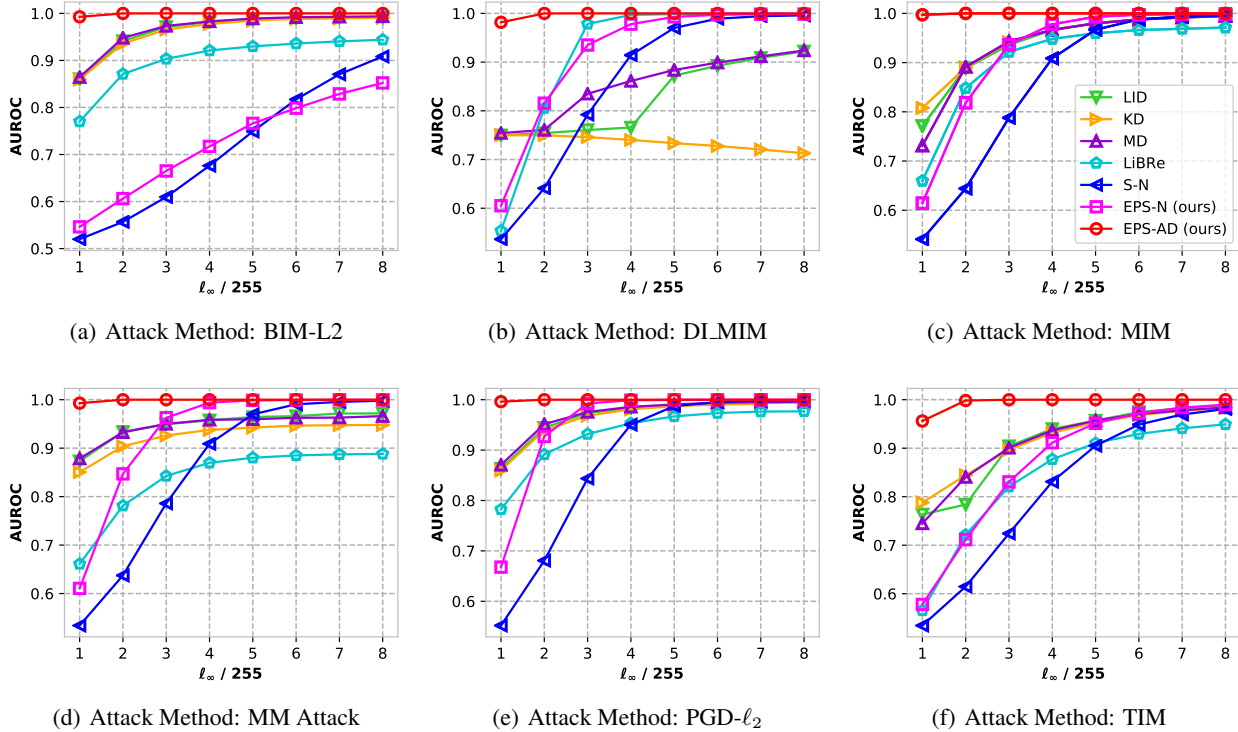


Figure 7. More Results of adversarial detection on ImageNet. Sub-figures (a) - (f) report the AUROC on different attacks under $\epsilon \in \{1/255, \dots, 8/255\}$ and share the same legend in sub-figure (c).

G.2. More Discussions of EPS-AD

Ablation of timestep. The ablation study of timestep is provided in Table 14 and Table 15. We observe that when the timestep $T > 10$, both EPS-AD and EPS-N obtain usable AUROC in detecting FGSM- ℓ_2 attack, which verifies that our method is insensitive to the timestep. Meanwhile, our methods consistently outperform the baseline S-N when $T > 20$, demonstrating the superiority of our methods. Moreover, Our approaches EPS-AD and EPS-N achieve optimum performance when $T^* = 20$ on CIFAR-10 and $T^* = 50$ on ImageNet, while the method S-N achieves optimum when $T^* = 5$ on CIFAR-10 and $T^* = 20$ on ImageNet.

Impact of set size. Previous adversarial detection methods usually measure the discrepancy well only with large amount of data (Gao et al., 2021). To show the effectiveness of our proposed EPS-AD, in this experiment, we further ablate the effect of set size by conducting experiments on 100 to 500 samples subset of CIFAR-10 with WideResNet-28-10 and ImageNet with ResNet-50. Performance of our three methods, S-N, EPS-N and EPS-AD, is shown in Table 16 and Figure 8. It is obvious that EPS-AD consistently outperforms EPS-N and S-N with small set size and large set size. Moreover, EPS-AD is robust to the changes of set size while EPS-N and S-N fluctuate with set size, especially on CIFAR-10 dataset.

Detecting on low attack intensity. To further reveal the superiority of our EPS-AD, we conduct an experiment under an extremely low attack intensity (e.g., $\epsilon = 1/255$) on ImageNet. In Table 21, our EPS-AD achieves a significant advantage in detecting adversarial samples crafted with extremely low attack intensity, demonstrating its significant effectiveness.

Detecting on adversarial samples across datasets. We further exploit the transferability across different datasets. To this end, we utilize a pre-trained score-based diffusion model on ImageNet to perform detecting adversarial samples from CIFAR-10. Specifically, we randomly select two disjoint subsets as adversarial and natural samples (each containing 500 samples) from CIFAR-10 and use a score model pre-trained on ImageNet to calculate the AUROC, which is named EPS-AD*. Table 22 demonstrates detection performance of 6 methods against 12 attacks under $\epsilon = 2/255$ on CIFAR-10 over WideResNet-28-10. We observe that EPS-AD* still exhibits superior detection performance compared to KD, LID, MD baselines, and achieves a comparable performance compared to other diffusion-based methods that use the score model pre-trained on CIFAR-10.

Table 10. Comparison of AUROC for using adversarial trained WideResNet-70-16 as classifier on CIFAR-10 under $\epsilon = 2/255$. Due to the constraint of memory and resources, we omit the detection results on AutoAttack for KD, LID and MD.

Method	KD	LID	MD	S-N	EPS-N (Ours)	EPS-AD (Ours)
FGSM	0.5852	0.7551	0.6924	0.9797	0.9976	0.9978
PGD	0.5672	0.7517	0.6846	0.9625	0.9954	0.9961
BIM	0.5786	0.7543	0.6787	0.9568	0.9935	0.9930
MIM	0.5795	0.7544	0.6804	0.9679	0.9963	0.9957
TIM	0.5812	0.7533	0.6783	0.8468	0.9506	0.9407
CW	0.5559	0.7511	0.6830	0.9600	0.9949	0.9953
DI-MIM	0.5763	0.7505	0.6712	0.8877	0.9728	0.9700
PGD- ℓ_2	0.6116	0.7632	0.7049	0.9942	0.9994	0.9998
FGSM- ℓ_2	0.6114	0.7619	0.7032	0.9471	0.9766	0.9861
BIM- ℓ_2	0.7550	0.7629	0.7060	0.9396	0.9756	0.9828

Table 11. Comparison of AUROC for using adversarial trained WideResNet-70-16 as classifier on CIFAR-10 under $\epsilon = 4/255$.

Method	KD	LID	MD	S-N	EPS-N (Ours)	EPS-AD (Ours)
FGSM	0.6020	0.7628	0.7668	0.9999	1.0000	1.0000
PGD	0.5913	0.7598	0.7535	0.9998	1.0000	1.0000
BIM	0.6076	0.7617	0.7588	0.9994	1.0000	1.0000
MIM	0.7683	0.7625	0.7601	0.9997	1.0000	1.0000
TIM	0.6029	0.7605	0.7563	0.9917	0.9984	0.9987
CW	0.5919	0.7581	0.7524	0.9998	1.0000	1.0000
DI-MIM	0.6015	0.7562	0.7551	0.9983	0.9998	0.9999
PGD- ℓ_2	0.8314	0.7774	0.7544	1.0000	1.0000	1.0000
FGSM- ℓ_2	0.7805	0.7709	0.7489	0.9803	0.9902	0.9967
BIM- ℓ_2	0.8351	0.7739	0.8141	0.9835	0.9927	0.9955

Results of EPS-AD with 5 different random seeds. We run our EPS-AD on CIFAR-10 and ImageNet against FGSM- ℓ_2 under $\epsilon = 4/255$ with 5 different random seeds and report the standard deviation of AUROC in Table 17. From the results, our EPS-AD has a very small standard error, indicating the consistency and repeatability of our methods.

Robustness of EPS-AD against adaptive attacks. To verify the robustness of our approach to adaptive attacks, we conduct the experiment on CIFAR-10 under PGD attack in a white-box setting, *i.e.*, both the classifier and the detector are available to the attacker. Specifically, we follow the strategy in Ma et al. (2018) to construct a modified attack objective: $\max \ell(\hat{f}(\hat{\mathbf{x}}), l) - \alpha \widehat{\text{MMD}}_b^2(\{\mathbf{x}^{(i)}\}_{i=1}^n, \{\hat{\mathbf{x}}\})$, where α is a constant balancing between the attack of the classifier and detector. When α increases, the attack successful rate (ASR) of PGD drops severely (when $\alpha = 0$, $ASR = 0.96$; when $\alpha = 1$, $ASR = 0.04$), indicating that the difficulty of attack increases significantly. Conversely, from Table 18, our EPS-AD achieves a high AUROC of 0.9154 even with a large $\alpha = 1$. The results demonstrate the robustness of our approach to adaptive attacks. The reason is that the minimization of the MMD between adversarial samples and natural samples gradually narrows the distributional discrepancy between natural and crafted adversarial samples, making it harder for the adversarial samples to mislead a trained classifier. This phenomenon is consistent with the discussion in Ma et al. (2018).

Inference efficiency of EPS-AD. Given a fixed-size model, the computational cost of our method (EPS-AD) mainly depends on two factors: the resolution of input images and total diffusion timestep T . Actually, our EPS-AD performs adversarial detection efficiently, especially on low-resolution images, and yields promising performance compared to existing methods. To evaluate the efficiency of EPS-AD, we randomly choose 500 images from CIFAR-10 and ImageNet respectively in detecting FGSM- ℓ_2 adversarial samples on a single RTX3090 GPU. The average time costs per image for CIFAR-10 ($T = 20$) and ImageNet ($T = 50$) are 0.043s and 2.369s, respectively.

To further demonstrate the effect of the resolution of input images and total diffusion timestep T on the efficiency, we provide the results of different resolutions of input images under different diffusion timesteps against FGSM- ℓ_2 attack. As shown in Table 20, our EPS-AD with resolution 256×256 shows superior adversarial detection performance when $20 \leq T \leq 100$ on ImageNet and takes 0.954s when $T = 20$, which is much more efficient than that with $T = 50$. When equipped with lower-resolution input size 128×128 , our EPS-AD stills keeps superior performance on ImageNet when

Table 12. Comparison of AUROC for using DeiT-S as classifier on ImageNet under $\epsilon = 4/255$.

Method	LID	S-N	EPS-N (Ours)	EPS-AD (Ours)
FGSM	0.8846	0.9789	0.9984	1.0000
PGD	0.9162	0.8935	0.9969	1.0000
BIM	0.9191	0.7331	0.9215	1.0000
MIM	0.9102	0.9025	0.9780	1.0000
TIM	0.9019	0.8091	0.8765	0.9606
CW	0.8742	0.8934	0.9975	0.9999
DI_MIM	0.7246	0.9074	0.9752	1.0000
PGD- ℓ_2	0.9041	0.9451	0.9987	1.0000
FGSM- ℓ_2	0.8698	0.7665	0.7023	1.0000
BIM- ℓ_2	0.9002	0.6564	0.6544	1.0000
MM	0.9164	0.8902	0.9886	0.9993
AA	0.9191	0.9023	0.9915	1.0000

 Table 13. Comparison with R-Rejection (Pang et al., 2022) on CIFAR-10 in terms of AUROC against FGSM under $\epsilon = 4/255$.

Method	PGD	PGD- ℓ_2	FGSM	FGSM- ℓ_2	BIM	BIM- ℓ_2	AA	MM
R-Rejection	0.9260	0.9420	0.8490	0.8690	0.7610	0.8390	0.8970	0.9080
EPS-N (Ours)	1.0000	1.0000	1.0000	0.9916	0.9996	0.9883	1.0000	0.9996
EPS-AD (Ours)	1.0000	1.0000	1.0000	0.9995	0.9998	0.9991	1.0000	0.9995

 Table 14. Impact of timestep with WideResNet-28-10 on CIFAR-10 against FGSM- ℓ_2 under $\epsilon = 4/255$.

Method \ timestep	1	2	5	10	20	50	100	200
S-N	0.9508	0.9792	0.9885	0.9860	0.9768	0.7590	0.6218	0.5597
EPS-N (Ours)	0.2346	0.4454	0.8018	0.9526	0.9916	0.9915	0.9889	0.9814
EPS-AD (Ours)	0.5166	0.5368	0.6994	0.9566	0.9994	0.9988	0.9985	0.9943
Method \ timestep	300	400	500	600	700	800	900	1000
S-N	0.5383	0.5274	0.5210	0.5172	0.5151	0.5147	0.5146	0.5144
EPS-N (Ours)	0.9766	0.9729	0.9705	0.9689	0.9680	0.9675	0.9672	0.9671
EPS-AD (Ours)	0.9921	0.9918	0.9910	0.9904	0.9896	0.9887	0.9878	0.9870

 Table 15. Impact of timestep with ResNet-50 on ImageNet against FGSM- ℓ_2 under $\epsilon = 4/255$.

Method \ timestep	1	2	5	10	20	50	100
S-N	0.4794	0.5298	0.7168	0.8528	0.8830	0.7309	0.5964
EPS-N (Ours)	0.2246	0.2466	0.4369	0.6215	0.7484	0.8191	0.8190
EPS-AD (Ours)	0.5112	0.5545	0.5662	0.6912	0.9917	1.0000	0.9930

$T = 50$ and only takes 0.780s. Moreover, in Table 19, the average time costs per image of our EPS-AD on CIFAR-10 with $T = 10$ and $T = 20$ are superior or comparable to existing methods (i.e., KD, LID, and MD), as well as the detection performance.

Note that the computational efficiency of our method can be further improved by applying an efficient sampling strategy (Lu et al., 2022), a low-resolution diffusion model (Dhariwal & Nichol, 2021) and a sparse diffusion timestep (e.g., sampling with a time interval of 2/1000 during the diffusion process). We leave these techniques for our future work.

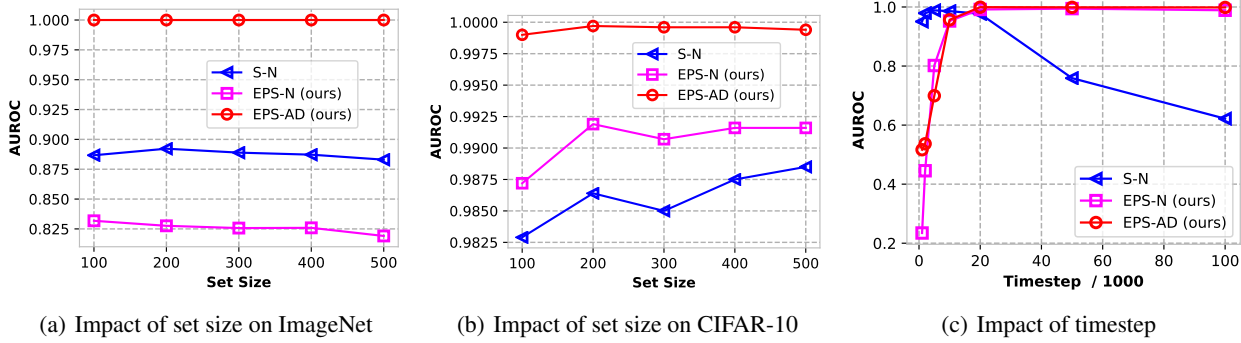


Figure 8. Impact of different set sizes and diffusion time step. Sub-figures (a) and (b) report the AUROC on FGSM- ℓ_2 attack under $\epsilon = 4/255$. Sub-figure (c) reports the AUROCs of different diffusion time in $\{1, 2, 5, 10, 20, 50, 100\}$ on CIFAR-10 dataset.

Table 16. Impact of data set size with WideResNet-28-10 on CIFAR-10 and ResNet-50 on ImageNet against FGSM- ℓ_2 under $\epsilon = 4/255$.

Dataset	size		100	200	300	400	500
	Method						
CIFAR-10	S-N		0.9829	0.9864	0.9850	0.9875	0.9885
	EPS-N (Ours)		0.9872	0.9919	0.9907	0.9916	0.9916
	EPS-AD (Ours)		0.9990	0.9997	0.9996	0.9996	0.9994
ImageNet	S-N		0.8867	0.8922	0.8889	0.8872	0.8830
	EPS-N (Ours)		0.8318	0.8276	0.8257	0.8259	0.8191
	EPS-AD (Ours)		1.0000	1.0000	1.0000	1.0000	1.0000

Table 17. Standard deviation of AUROC with 5 different random seeds over WideResNet-28-10 on CIFAR-10 and ResNet-50 on ImageNet against FGSM- ℓ_2 under $\epsilon = 4/255$.

Dataset	CIFAR-10	ImageNet
PGD	1.0000 ± 0	$0.9999 \pm 4 \times 10^{-5}$
FGSM	1.0000 ± 0	1.0000 ± 0
BIM	$0.9999 \pm 8.94 \times 10^{-5}$	1.0000 ± 0
MIM	1.0000 ± 0	1.0000 ± 0
TIM	$0.9996 \pm 1.67 \times 10^{-4}$	$0.9999 \pm 1.26 \times 10^{-4}$
DLMIM	$0.9999 \pm 4 \times 10^{-5}$	1.0000 ± 0
CW	1.0000 ± 0	$0.9999 \pm 4 \times 10^{-5}$
PGD- ℓ_2	1.0000 ± 0	1.0000 ± 0
FGSM- ℓ_2	$0.9996 \pm 2.45 \times 10^{-4}$	1.0000 ± 0
BIM- ℓ_2	$0.9992 \pm 2.97 \times 10^{-4}$	1.0000 ± 0
MM	$0.9967 \pm 3.08 \times 10^{-3}$	1.0000 ± 0
AA	$0.9997 \pm 6.4 \times 10^{-4}$	1.0000 ± 0

Table 18. AUROC of EPS-AD under different α against an adaptive attack (PGD) under $\epsilon = 4/255$ on CIFAR-10.

Method \ α	0	10^{-7}	10^{-6}	10^{-5}	10^{-4}	10^{-3}	10^{-2}	10^{-1}	1
EPS-AD (Ours)	1.0000	0.9859	0.9681	0.9353	0.9303	0.9284	0.9168	0.9145	0.9154

Table 19. Results of adversarial detection performance (AUROC & time costs per image) against FGSM- ℓ_2 attack ($\epsilon = 4/255$) under different total diffusion timesteps on CIFAR-10.

Dataset	KD	LID	MD	Timestep	EPS-AD
CIFAR-10				$T = 5$	0.6994 (0.021s)
				$T = 10$	0.9566 (0.028s)
			0.9995	$T = 20$	0.9995 (0.043s)
				$T = 50$	0.9988 (0.090s)
				$T = 100$	0.9985 (0.168s)

Table 20. Results of adversarial detection performance (AUROC & time costs per image) against FGSM-L2 attack ($\epsilon = 4/255$) under different total diffusion timesteps on ImageNet, where “EPS-AD (128 × 128)” and “EPS-AD (256 × 256)” denote EPS-AD with different resolution inputs.

Dataset	KD	LID	MD	LiBRe	Timestep	EPS-AD (128 × 128)	EPS-AD (224 × 224)
ImageNet	0.7004 (0.029s)	0.8932 (0.020s)	0.8715 (0.069s)	0.8708 (0.029s)	$T = 5$	0.4652 (0.112s)	0.5662 (0.268s)
					$T = 10$	0.6385 (0.187s)	0.6912 (0.498s)
					$T = 20$	0.7501 (0.335s)	0.9917 (0.992s)
					$T = 50$	0.9991 (0.780s)	1.0000 (2.369s)
					$T = 100$	0.9392 (1.519s)	0.9930 (4.696s)

Table 21. Comparison of different adversarial detection methods with attack intensity $\epsilon = 1/255$ over ResNet-50 on ImageNet.

Method	KD	LID	MD	LiBRe	S-N	EPS-N (Ours)	EPS-AD (Ours)
FGSM	0.7301	0.7765	0.7694	0.5653	0.5654	0.6942	0.9982
PGD	0.8167	0.7651	0.8116	0.6938	0.5348	0.6149	0.9637
BIM	0.8313	0.7711	0.8303	0.7154	0.5240	0.5619	0.9845
MIM	0.8079	0.7711	0.7313	0.6597	0.5411	0.6144	0.9972
TIM	0.7879	0.7634	0.7449	0.5655	0.5344	0.5780	0.9561
CW	0.8161	0.7690	0.8336	0.6996	0.5345	0.6169	0.9549
DL-MIM	0.7498	0.7498	0.7543	0.5538	0.5364	0.6052	0.9817
PGD- ℓ_2	0.8597	0.8633	0.8707	0.7824	0.5519	0.6678	0.9961
FGSM- ℓ_2	0.7265	0.7737	0.7704	0.5727	0.5546	0.5978	0.9997
BIM- ℓ_2	0.8596	0.8602	0.8644	0.7701	0.5199	0.5462	0.9927
MM	0.8505	0.8730	0.8786	0.6611	0.5340	0.6106	0.9928
AA	0.8535	0.8706	0.8733	0.6629	0.5351	0.6113	0.9936

Table 22. Comparison of cross-dataset EPS-AD* under attack intensity $\epsilon = 2/255$ with other methods over WideResNet-28-10 on CIFAR-10, where EPS-AD* utilizes a score model pre-trained on ImageNet.

Method	KD	LID	MD	S-N	EPS-N (Ours)	EPS-AD (Ours)	EPS-AD*
PGD	0.8871	0.8836	0.8815	0.9679	0.9950	0.9972	0.9987
FGSM	0.9112	0.9010	0.9200	0.9902	0.9987	0.9994	0.9961
BIM	0.8786	0.8878	0.8811	0.9268	0.9811	0.9914	0.9890
MIM	0.8873	0.8909	0.8947	0.9676	0.9935	0.9975	0.9964
TIM	0.8983	0.8735	0.9655	0.9603	0.9878	0.9747	0.9906
CW	0.8634	0.8762	0.8968	0.9682	0.9953	0.9975	0.9971
DL-MIM	0.7810	0.7351	0.8153	0.9348	0.9764	0.9942	0.9918
PGD- ℓ_2	0.8727	0.8935	0.9128	0.9931	0.9989	0.9997	0.9994
FGSM- ℓ_2	0.9044	0.8927	0.9211	0.9166	0.9634	0.9976	0.9973
BIM- ℓ_2	0.8675	0.8864	0.8946	0.8564	0.9333	0.9922	0.9896
MM	0.8627	0.8843	0.8404	0.9497	0.9706	0.9727	0.9658
AA	0.8754	0.8894	0.8392	0.9595	0.9775	0.9819	0.9782